Precambrian Research 252 (2014) 88–106

Contents lists available at ScienceDirect

Precambrian Research

journal homepage: www.elsevier.com/locate/precamres

Paleoenvironmental implications of two phosphogenic events in Neoproterozoic sedimentary successions of the Tandilia System, Argentina

Lucía E. Gómez-Peral[a,*], Alan J. Kaufman[b], Daniel G. Poiré[a]

[a] Centro de Investigaciones Geológicas, CONICET-UNLP, Argentina
[b] Department of Geology and Earth System Science Interdisciplinary Center, University of Maryland, United States

ARTICLE INFO

Article history:
Received 27 December 2013
Received in revised form 1 June 2014
Accepted 14 July 2014
Available online 27 July 2014

Keywords:
Phosphate concretions
REE
Sierras Bayas Group
Neoproterozoic
Río de La Plata Craton

ABSTRACT

Two phosphogenic events of potential economic importance (preserving P_2O_5 abundances up to 25 and 35%, respectively) are recognized in the Neoproterozoic Tandilia System. The older of the two lies atop a quartz-arkosic facies association of the Villa Mónica Formation. The age of this unit remains controversial, but has previously been considered as Tonian to Cryogenian based on stromatolite assemblages and carbon isotope trends; strontium isotope abundances of <0.7071 currently support an earliest Cryogenian age for the formation. The younger phosphate level lies at the base of the Cerro Negro Formation above a widespread karstic surface in a succession containing *Cloudina*, so is most-likely to be Ediacaran in age. In both cases, the phosphatic concretionary levels are related to relative sea-level fall and exposure that may be related to glacial eustacy. In order to reconstruct the paleoenvironment associated with the formation of these concretionary phosphates, we combined field observations with thin-section petrography, XRD, SEM and geochemical analyses. Total rare-earth element (REE) contents range from 311 to 1010 ppm in concretions from the Villa Mónica Formation and from 290 to 1471 ppm those from the Cerro Negro Formation. Villa Mónica concretions reveal no anomalies in Ce abundance, but clearly positive Eu anomalies (ranging from 1 to 1.4). These results suggest reduced conditions in the marine depositional environment. In contrast, Eu anomalies are not recorded in Cerro Negro concretions, while negative Ce anomalies, ranging from −0.14 to −0.18, are noted. These results are consistent with oxic seawater conditions in mixed platform facies. This study suggests that depositional conditions where phosphate was concentrated in the Neoproterozoic Tandilla System were markedly different.

1. Introduction

Although the processes of Phanerozoic phosphorite accumulation are generally well understood, the environmental conditions that resulted in the accumulation of Proterozoic phosphorites remain largely unresolved. In part, this is due to the greater abundance and economic importance of Phanerozoic deposits relative to those of the Proterozoic (Baioumy, 2011). Thus, fewer studies have documented the extent and biogeochemical implications of Proterozoic phosphorites (e.g., Melezhik et al., 2005), nor their potential relationship to biological innovations or paleoclimatic events. For example, Ediacaran and Early Cambrian phosphogenic event may have promoted the sudden appearance of animals and the onset of biomineralization. To address the need for further study, we have focused on two levels of phosphate concretions preserved in the Neoproterozoic Sierras Bayas Group (~850–541 Ma) on the Rio de la Plata Craton of Argentina.

The Sierras Bayas Group is composed of terrigenous clastic as well as marine peritidal to subtidal clastic and chemical sedimentary rocks. The first phosphatic level in the group occurs in the lower reaches of the Villa Mónica Formation and the second unconformably overlies the Loma Negra Formation in the basal Cerro Negro Formation. The physical and chemical conditions that produced phosphorite concretions in the Sierras Bayas Group may be understood through the reconstruction of depositional environments, with the aim of relating the phosphatic lithofacies to physical and chemical sedimentary processes.

Phosphorite formation through time is recognized as episodic, but when it occurs it appears to be of global extent (Cook and McElhinny, 1979; Bentor, 1980; Sheldon, 1980, 1981; Cook and Shergold, 2005; Xiao et al., 2012). Minor episodes of Neoproterozoic

* Corresponding author. Tel.: +54 221 4215677; fax: +54 221 4258696.
E-mail addresses: lperal@cig.museo.unlp.edu.ar, luciagomezperal@gmail.com (L.E. Gómez-Peral).

http://dx.doi.org/10.1016/j.precamres.2014.07.009
0301-9268/

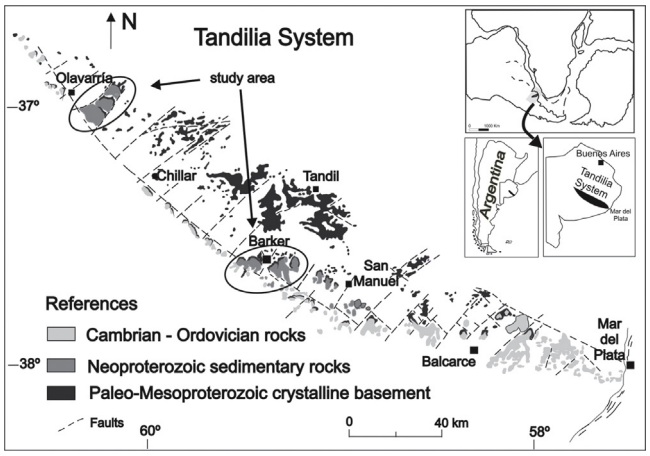

Fig. 1. Study areas in the Tandilia System (Buenos Aires Province, Argentina).

phosphogenesis appear in Cryogenian successions (currently constrained between 850 and 635 Ma) while a major event is preserved in middle Ediacaran (between 635 and 541 Ma) strata, especially well developed in South China (Notholt et al., 1989; Cook and Shergold, 2005; Xiao et al., 2012). In Argentina, only one occurrence in the Cerro Negro Formation has previously been reported (Leanza and Hugo, 1987); here we include a newly recognized horizon at the base of the Villa Monica Formation. Previous authors have suggested a strong correlation between major phosphogenic events and relative sea-level changes (Vail et al., 1977; Cook and McElhinny, 1979; Tissot, 1979; Sheldon, 1980; Cook, 1992; Cook and Shergold, 2005), which we consider here as a model for the Tandilla System.

Oceanic upwelling is considered by many to be the most-likely mechanism to explain the origin of phosphorite in marine sediments. This model implies that the rise of cold nutrient-rich deep water toward the shallow platform resulted in high primary productivity and the sequestration of phosphorous-rich organic matter in sediments in the shallowest marine zone (Wright et al., 1984, 1987; Grandjean et al., 1987, 1988; Bertram et al., 1992; Misi and Kyle, 1994; Jarvis et al., 1994; Ilyin, 1998; Yang et al., 1999; Mazumdar et al., 1999; Chen et al., 2003). The phosphate concretions observed in Tandilia System strata are associated with chert, iron formation, and organic-rich carbonates, which are consistent with transgression, oceanic upwelling, and enhanced organic productivity. Rocks of the Sierras Bayas Group and Cerro Negro Formation, including the thin (<1 m) phosphate rich horizons, are little deformed and well preserved. In this study we evaluate the phosphorites in light of the physical stratigraphy of the successions and their paleogeographic position along the southwest margin of Gondwanaland, and combine new REE measurements of the phosphorite concretions with carbon, oxygen, and strontium isotope data (Knoll et al., 1986; Kaufman et al., 1993, 1996) from host lithologies to better understand the depositional and diagenetic processes related to their genesis.

2. Geological setting

The Tandilia System is a 350 km long, northwest–southeast oriented orographic belt located in Buenos Aires Province of Argentina (Fig. 1). It comprises an igneous-metamorphic basement covered by Neoproterozoic to lower Paleozoic sedimentary rocks. The basement rocks are mainly granitoids, orthogneisses and migmatites of the Buenos Aires Complex yielding U–Pb SHRIMP ages between 2234 and 2065 Ma (Cingolani et al., 2002; Hartmann et al., 2002; Cingolani, 2011), and Sm–Nd model ages averaging around 2620 ± 80 Ma (Pankhurst et al., 2003). The Buenos Aires Complex (Marchesse and Di Paola, 1975) is composed of granitoids, migmatites, mylonites, amphibolites and basic dykes (Cingolani and Dalla Salda, 2000). The main tectonomagmatic event in Tandilia is of Transamazonian age (ca. 2.2–2.1 Ga, Hartmann et al., 2002; Cingolani et al., 2002). Detrital zircon U–Pb ages indicate a Paleoproterozoic to Mesoproterozoic source of clastic material in the Neoproterozoic succession (Rapela et al., 2007; Gaucher et al., 2008; Cingolani, 2011). Gaucher et al. (2008) and Cingolani (2011) observe an obvious change in detrital provenance from the Villa Mónica to the Cerro Largo and Cerro Negro formations (see also Zimmermann et al., 2011 who provide geochemical evidence for a change in procenance).

In the Olavarría-Barker area (Fig. 1) the overlying Neoproterozoic sedimentary succession, which is little deformed and reveals no obvious evidence of burial metamorphism, is composed of the Villa Mónica, Colombo, Cerro Largo, Olavarría and Loma Negra formations (Sierras Bayas Group ~185 m), which are overlain unconformably by the Cerro Negro Formation (Fig. 2). Between the crystalline basement and the Neoproterozoic sedimentary cover, arkosic and quartz-kaolinitic gruss mark prominent paleoweathering surfaces (Poiré, 1987; Zalba et al., 1992). The lithostratigraphic units are grouped into five depositional intervals representing either unconformity bounded sequences or parasequences bounded by flooding surfaces (Fig. 2): Tofoletti (I), Malegni (II), Diamante (III), Villa Fortabat (IV) and La Providencia (V) (Spalletti and Poiré, 2000; Poiré and Spalletti, 2005; Poiré, 2012b).

The oldest unconformity bounded sequence (Tofoletti, 52–70 m thick; Figs. 2 and 3) exhibits two sedimentary facies associations: quartz-arenite and arkosic sandstone at the base, and dolostone including shallow marine stromatolites and shale-marl at the top. Sandstones of the Villa Mónica Formation have a unimodal zircon population of Transamazonia affinity, with a peak age at 2.15 Ga and a subordinate population of grains at 1.0 Ga (Rapela et al., 2007; Gaucher et al., 2008). The quartz-arkosic facies association (Poiré, 1987) marks the beginning of a transgressive systems tract. This siliciclastic succession is 16–21 m thick and shows at the top the presence of shale facies with thin sandstone levels and phosphate concretions with associated mudstone lenses (Gómez-Peral et al., 2011). These authors indicate a meso-diagenetic overprint followed by an uplift and telo-diagenetic modification. The dolostone and shale facies (36–52 m thick) are composed of laminated stromatolitic dolostones, interbedded green shales and overlaying red shales with associated mudstones. Near the base of the dolostone facies, abundant phosphorite clasts were recognized in the inter-stromatolite fill.

The dolostones of the Villa Mónica Formation host a rich assemblage of stromatolites, including *Colonnella* fm., *Conophyton resotti*, *Conophyton* fm., *Cryptozoon* fm., *Gongylina* fm., *Gymnosolen* fm., *Inzeria* fm., *Jacutophyton* fm., *Jurusonia* cf. *nisvensis*, *Katavia* fm., *Kotuikania* fm., *Kussiella* fm., *Minjaria* fm., *Parmites* fm., *Parmites* cf. *concrescens* and *Stratifera* fm. (Poiré, 1993, 2012a; Gaucher and Poiré, 2009a). Acritarchs reported from the Villa Mónica Formation (Gaucher et al., 2005) consist mainly of large (up to 450 μm) leiosphaerids.

The erosional surface above the Villa Mónica Formation is marked by a karst (Piedra Amarilla surface) followed by breccias and diamictites of the Colombo Formation (Gómez-Peral et al., 2011, 2012). The basal diamictite (Gaucher and Poiré, 2009b) contains blocks up to 3 m in diameter (i.e., sandstone, shale, dolostone and chert breccia), synsedimentary deformation structures, and a sandstone-mudstone matrix (Gómez-Peral et al., 2011). At this contact, Rapalini et al. (2013) assigned a tentative age for the telodiagenesis of 590 Ma on the basis of paleomagnetic data. Above the diamictite, finely laminated glauconitic shales and fine-grained sandstones appear in the basal part of the Cerro Largo Formation.

Deposicional Sequence		Formation	Facies association	fossil content	thickness	Palaeoenvironment	Age
La Providencia		**Cerro Negro**	heterolithic facies marls chert-**phosphates**	*Skolithos* acritarchs	+200 m	Intertidal flat Transgressive shallow marine	Late Ediacaran
Barker surface							
Sierras Bayas Group	Villa Fortabat	**Loma Negra**	micritic mudstones	*Cloudina* *Helminthopsis*	24-42 m	Carbonate ramp to restricted platform or lagoon	$\delta^{13}C$ $^{87}Sr/^{86}Sr$ ~ 580 Ma (Gómez Peral *et al.*, 2007) 560-543 Ma (Gaucher and Poiré, 2009)
	Diamante	**Olavarría**	siltstones and claystones	acritarchs	35 m	Transgressive system track at the base. Tidal influence and storm deposits	-
	Malegni	**Cerro Largo**	quartz arenites	biofilms	+/-25 m	subtidal sandy flat	-
			sandstones and shales	acritarchs	15 m	Highstand to lowstand marine stable platform	-
		Colombo	shales, chert breccias, diamictites		3-8 m	subaerial exposure	-
Piedra amarilla surface							
	Tofoletti	**Villa Mónica**	dolostones	stromatolites	36-52 m	supratidal stromatolitic platform	stromatolites 800-900 Ma (Poiré, 1987) $\delta^{13}C$ $^{87}Sr/^{86}Sr$ Cryogenian (Gómez Peral *et al.*, 2007)
			chert - iron formation -**phosphates** arenites, wakes,conglomerates	acritarchs	22 m	Lowstand to highstand marine	-
Buenos Aires Complex - Igneous-metamorphic basement							Paleoproterozoic ~ 2200 Ma

Fig. 2. Stratigraphic and sequential table of the Precambrian – lower Paleozoic sedimentary cover of the Tandilia System (Poiré and Spalletti, 2005; after Gómez-Peral et al., 2011, modified).

The upper part of this unit consists of cross-bedded quartz sandstones with sigmoidal, herringbone and hummocky cross-stratification (Gómez-Peral et al., 2011). This succession represents a shallowing-upward succession, ranging from subtidal nearshore to tidal-flat deposits (Poiré, 1987).

The overlying Diamante sequence (Olavarría Formation) is approximately 35 m thick and includes a transitional basal contact represented by quartzite to mudstone heterolithic facies, showing a transition from flaser through wavy to lenticular bedding. It is composed of mudstone and heterolithic facies with 8–20 cm concretionary beds very rich in iron oxides. At the top of the sequence (i.e., red mudstones and shales), carbonate concretions were recognized (Gómez-Peral et al., 2011). This sequence is equivalent to the Las Águilas Formation (Andreis et al., 1996) in the central part of the Tandilia System in the Barker area (Figs. 1 and 2) (Poiré and Spalletti, 2005), where it is represented by silt- and iron-rich claystones with an acritarch assemblage consisting of *Paleorivularia ontarica*, *Chuaria olavarriensis* and *Leiosphaeridia* sp. (Pöthe de Baldis and Cuomo, 1983). These fossils were re-interpreted by Gaucher et al. (2005) as representing the taxa *Chuaria circularis*, *Leiosphaeridia minutissima* and *Synsphaeridium* sp.

The youngest depositional sequence of the Sierras Bayas Group is known as Villa Fortabat (Figs. 2 and 3), which is represented by 40 m almost exclusively composed of reddish or greenish (lower section) and black (upper section) micritic limestones originated by suspension fall-out in open marine ramp and lagoon environments. This sequence is equivalent to the Loma Negra Formation (Poiré, 1993). The trace fossil *Helminthopsis* isp. and probable medusa resting traces have been recorded (Poiré et al., 2003). Cloudina riemkeae, an index fossil for the upper Ediacaran Period has been described by Gaucher et al. (2005) from limestones of the Loma Negra Formation. The combined biogeochemical features (C and S isotopes and hydrocarbon biomarkers) of the Loma Negra Formation in the Barker area (Fig. 1) suggest a well-stratified water column with oxygenated surface waters, oxygen-poor bottom waters and anoxic sediments. These paleontological and biogeochemical features are common to the Polanco Formation from the Arroyo del Soldado Group in Uruguay (Bagnoud-Velásquez et al., 2013) supporting the exact correlation of these units.

Finally, the Sierras Bayas Group is overlain by the Cerro Negro Formation with erosional unconformity (Barrio et al., 1991). This surface has been related to a eustatic sea-level fall (Poiré et al., 2007) although evidence of glaciation at this level is absent. Erosion and the meteoric dissolution of the carbonate sediments formed a karst surface onto which residual clays and brecciated chert were deposited (Barrio et al., 1991). Furthermore, phosphate concretions are common at this level, which resulted from the recrystallization of amorphous phosphate to apatite (Leanza and Hugo, 1987). The Cerro Negro Formation (La Providencia depositional sequence; Figs. 2 and 3) exceeds 150 m in thickness and is characterized by claystone and heterolithic, fine-grained sandstone-claystone intercalations, mainly formed in upper to lower tidal flats. *Skolithos*-bearing marl and mudstone (Fig. 3) compose the lower part of the unit (Poiré et al., 2003) suggesting a Cambrian age for the unit. Acritarchs reported by Cingolani et al. (1991) consist of simple forms of sphaeromorphs, such as *Synsphaeridium* sp., *Trachysphaeridium* sp. and *Leiosphaeridia* sp.

Existing geochronological constraints for the Sierras Bayas Group are sparse and controversial. The age of the Villa Mónica Formation was originally considered to be Tonian or Cryogenian in age based on stromatolite biostratigraphy (e.g., Semikhatov, 1975, 1991; Poiré, 1989, 1993). This temporal assignment is broadly supported by a 793 ± 32 Ma Rb/Sr age from interbedded fine-grained sedimentary rocks (Cingolani and Bonhomme, 1988), but it most likely represents a diagenetic overprint. Gómez-Peral et al. (2007) later suggested a Cryogenian affinity for the unit based on a muted negative-to-positive trend in carbon isotopes that mimics those in post-glacial cap carbonates. Our new strontium isotope measurements of calcitic samples of the dolostones of Villa Mónica Formation, which range narrowly from 0.7069 to 0.7071, are similar

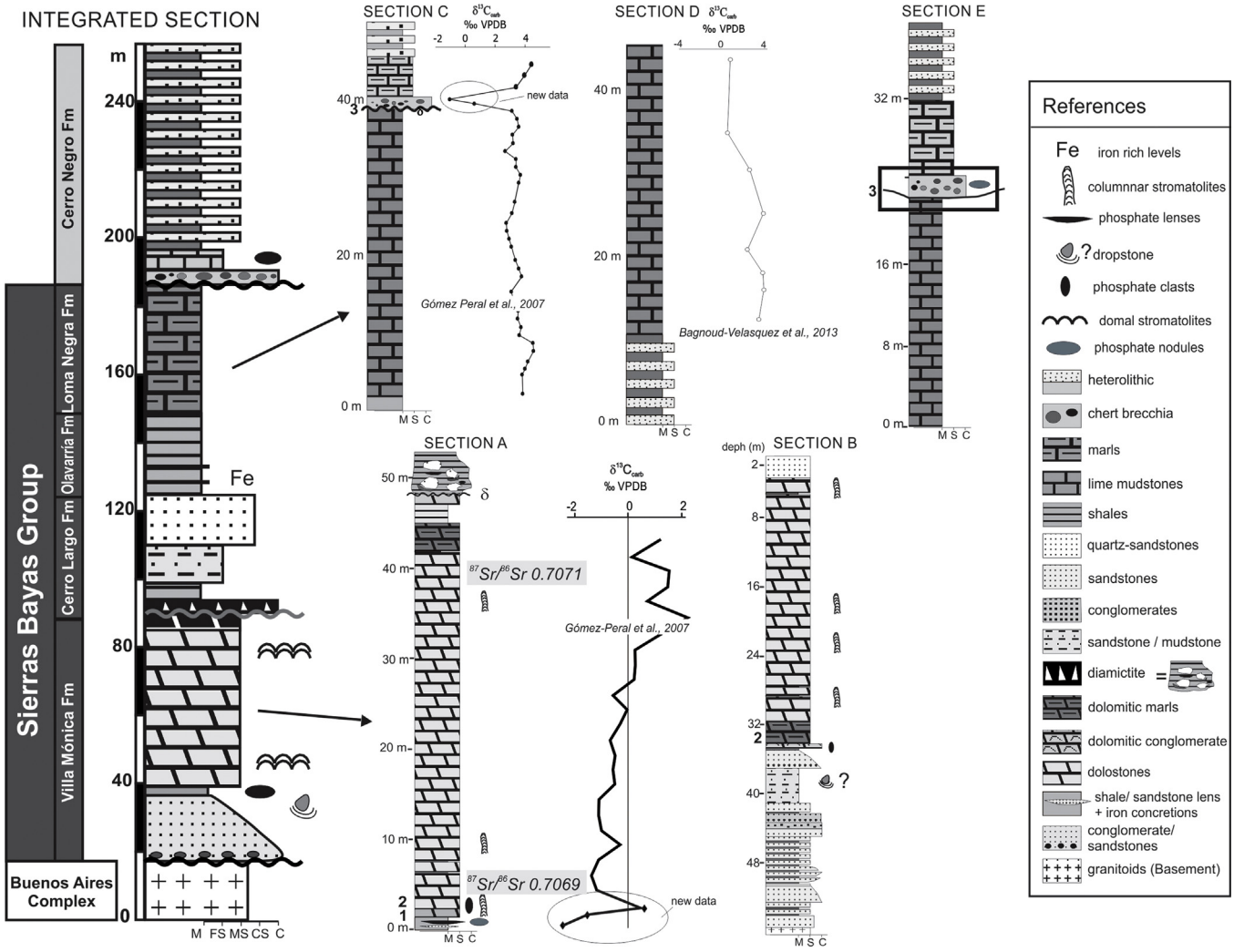

Fig. 3. Integrated section: Schematic representation of the Sierras Bayas Group and Cerro Negro Formation. Section A: Piedra Amarilla Quarry; Section B: El Polvorín Quarry (drill core); Section C: Cementos Avellaneda Quarry (Olavarría; Gómez-Peral et al., 2007); Section D: Villa Cacique Quarry (Barker; Bagnoud-Velásquez et al., 2013); Section E: Portcecal Quarry. References: BAC = Buenos Aires Complex; VMF = Villa Mónica Formation; CLF = Cerro Largo Formation; OF = Olavarría Formation; LNF = Loma Negra Formation; CNF = Cerro Negro Formation.

to those (Kaufman et al., 1996, 2009) that span the (>746 Ma) Chuos glacial diamictite in the Otavi Group of northern Namibia (Hoffman et al., 1996). This ice age deposit may be representative of the oldest of the Cryogenian glacial events and thus may provide a lithostratigraphic marker for the base of the period. However, insofar as the Villa Mónica carbonates are mostly dolomitic, it is possible that the $^{87}Sr/^{86}Sr$ compositions in our selected samples have been reset to slightly higher values. If correct, a pre-Cryogenian Tonian age is most likely for this formation. Detrital zircons in sandstones of the Cerro Largo Formation are characterized by a dominant Transamazonian zircon population with peaks at 2.15, 2.0 and 1.78 Ga, but also display Archean to earliest Paleoproterozoic (3.33, 2.99, 2.7, 2.46 Ga) and Mesoproterozoic peaks (1.55, 1.23 and 1.05 Ga) (Gaucher et al., 2008). Regarding the Loma Negra Formation, Gaucher et al. (2005) reported the occurrence of *Cloudina* cf. *C. riemkeae* in the muddy limestones, which implies an age of ca. 560–543 Ma (Gaucher and Poiré, 2009a). This makes it possible to correlate the $\delta^{13}C$ excursions (+2 to +4‰) and Sr isotope data (0.7070–0.7080, Kawashita et al., 1999) recorded for the Loma Negra Formation with those from the Polanco Formation (Uruguay) and Corumbá Group (Brazil), which are similarly constrained to be around 560 Ma in age (Gómez-Peral et al., 2007; Blanco et al., 2009; Gaucher et al., 2009; Gaucher and Germs, 2009; Boggiani et al., 2010). The age of the Cerro Negro Formation is currently under debate; on one hand the bioturbation related to *Skolithos* suggests a Cambrian affinity, while on the other the acritarch assemblage supports a late Ediacaran designation (Gaucher et al., 2005).

It is important to highlight the two major stratigraphic discontinuities in the Sierras Bayas Group, including the lower surface at the contact between the Villa Mónica and Cerro Largo formations (the "Piedra Amarilla Surface"), and the upper surface on top of the Loma Negra Formation (the "Barker Surface"). The latter may have been expressed worldwide and related to glacial eustacy insofar as it has been correlated with other Neoproterozoic omission surfaces in Uruguay, Brazil, South Africa and Namibia (Poiré et al., 2007; Praekelt et al., 2008; Germs and Gaucher, 2012). Both of the Sierras Bayas unconformities are associated with the development of karst on carbonate lithologies filled with diamictite, chert and phosphate concretions, and intra-formational breccia (Fig. 2). On the other hand, the transitional or planar contacts between the Cerro Largo and Olavarría formations, and the Olavarría and Loma Negra formations reflect variations in paleoenvironmental conditions, recognized primarily by pronounced lithological changes (Fig. 3).

Table 1
XRD semiquantitative results in whole rock and clay fraction analysis from the Villa Mónica (CO, T6) and Cerro Negro formations (PR and M). pl = phosphate lens; pc = phosphate concretion; pcld = phosphatic clasts in dolostones; pcl = phosphatic clast; ps = purple shale; s = sandstone; il = iron level; gs = green shale; d = dolostone; pm = phosphate with marl matrix; rs = red shale; m = marl.

Sample	Quarry	Lithology	X ray diffraction														
			Whole rock									Clayminerals					
			Qz	F	C	Ca	D	Fap	Gt	I	I/S	C	C/S	Sm	K	Py	IC	IE
Villa Mónica Fm																	
Col 1	Piedra amarilla	Purple shale	va	vs	m	–	–	–	–	90	10	–	–	Tr	–	–	0.5	0.32
Col 2	Piedra amarilla	Purple shale	va		m	–	–	s	–	55	20	3	8	2	12		0.6	nc
Col 3	Piedra amarilla	Shale	va	vs	m	–	–	–	–	90	10	–	–	–	–	–	0.4	0.32
COL 5B	Piedra amarilla	Green shale	a	vs	s	a	–	m	–	85	10	5	–	–	–	–	0.52	0.25
CO.5	Piedra amarilla	Iron level	va	vs	vs	s	–	–	s	70	10	20	–	–	–	–	nc	nc
CO.1	Piedra amarilla	Phosphate concretion	a	vs	s	–	–	a	–	85	10	–	–	5	–	–	0.63	0.36
CO.2	Piedra amarilla	Phosphate lens	a	vs	vs	–	–	a	–	n.i.								
CO.3	Piedra amarilla	Phosphate lens	va	Tr	s	–	–	a	–									
CO.4	Piedra amarilla	Phosphate lens	m	–	s	–	–	va	–									
CO.6	Piedra amarilla	Green shale	va	vs	m	m	–	–	–									
T6 32.55	El Polvorín	Dolostone	m	vs	vs	vs	va	s	–	77	15	–	–	–	–	8	nc	nc
T6 33.85 D	El Polvorín	Phosphatic clast	a	–	vs	vs	a	m	–	58	20	12	5	–	5	–	nc	nc
T6 33.85 F	El Polvorín	Phosphatic clast	m	–	vs	–	–	va	–	85	15	–	–	–	–	–	0.4	0.36
Cerro Negro Fm																		
PR 3	Portcecal	Phosphate concretion	a	–	Tr	–	–	va	–	n.i.								
M3b	Portcecal	Phosphate marl matrix	va	vs	vs	m	–	s	–									
PR 1	Portcecal	Phosphate concretion	a	–	vs	–	–	va	–									
PR 2	Portcecal	Phosphatic clast	m	–	s	–	–	va	–	80	10	10	–	–	–	–	nc	nc
M4	Portcecal	Red shale	va	s	s	s	–	–	–	70	–	5	15	–	10	–	0.40	0.38
M5	Portcecal	Marl	a	vs	vs	va	–	–	–	85	10	Tr	5	–	–	–	0.43	0.40
M6	Portcecal	Red shale	va	vs	s	s	–	–	–	90	10	–	–	–	–	–	0.48	0.4

Qz: quartz, F: feldpars, C: clay, Ca: calcite, D: dolomite, Fap: fluorapatite, Gt: goethite, Tr: <1%, vs: 1–5%, s: 5–15%, m: 15–30%, a: 30–50%, va: 50–100%, nc: non qunatified, Sm: esmectite, Cl: chlorite, I/S: interestratified illite–esmectite, Cl/S: interestratified chlorite–esmectite, I: illite, K: kaolinite, Py: pyrophyllite, IC: illite crystallinity index; IE: Esquevin index.

2.1. Phosphate horizons

The lower of the two phosphatic horizons recognized in the Tandilia System (Fig. 1) occurs in the Villa Mónica Formation, where phosphate concretions are interbedded with shale near the base of the unit. Immediately above the shale, a centimeter-thick conglomerate containing reworked phosphate clasts in a dolomite matrix is observed and overlain by columnar and stratiform stromatolites. The younger phosphate horizon at the base of the Cerro Negro Formation immediately above an unconformity is composed of phosphatic and chert concretions in either a laminated shale or mudstone matrix. The concretions at both levels are composed of black and dark gray fluorapatite associated with quartz and a variety of clay minerals (Table 1).

2.1.1. Villa Mónica phosphate level

In the Piedra Amarilla Quarry (Fig. 1), phosphate lenses and concretions are associated with laminated shales, ironstone (goethite) and red colored chert. The phosphate nodules have planar shapes elongated (up to 12 cm wide × 12 cm long × 6 cm thick) parallel to laminations, while the stratiform lenses are up to 40 cm long. Reworking of phosphate lenses most likely resulted in clasts that are concentrated in the overlying conglomerate at the base of the dolomitic shale facies. Clasts were concentrated and sorted by size and hardness (i.e., phosphate, quartz and, less frequently, mudstone clasts) in parts of the carbonate platform exposed to strong currents or surges. The bedded conglomerate is 60 cm thick on average and it also creates fill between columnar stromatolites. Similar features are identified in drill core samples from El Polvorín Quarry (Fig. 3). The clasts are prolate and laminated, varying in size from a few millimeters to 3.5 cm and in most cases with their major axes perpendicular or oblique to stratification. They are subrounded to subangular and surrounded by iron-rich dolomitic cement.

2.1.2. Cerro Negro phosphate level

The upper phosphate level of the Cerro Negro Formation was first recognized by Leanza and Hugo (1987). These authors interpreted this level to have originated as a result of the filling of a channelized paleosurface, with development of channels on top of the Loma Negra Formation due to sea-level regression. At the base of the Cerro Negro Formation, phosphate nodules and lenses are concentrated in a marl-rich matrix associated with residual green claystones and very large cherty concretions (up to 2–3 m in diameter), which are evenly distributed in the karstic channels (Fig. 3). In the Portcecal Quarry, located in the northern Sierras Bayas Hill (Fig. 1) phosphate concretions in the paleokarst surface have also been recognized.

3. Sampling and methodology

Three detailed profiles located in the Piedra Amarilla, Portcecal and El Polvorín quarries (Figs. 1 and 3) were surveyed and sampled in detail (see Tables 1–3). Phosphate samples from the Villa Mónica Formation ($n = 23$) were collected from the Piedra Amarilla Quarry, located near the city of Sierras Bayas, and from drill cores at El Polvorín quarry. Samples of phosphatic concretions from the Cerro Negro Formation ($n = 10$) were collected at the Portcecal Quarry near Olavarría, and Villa Cacique Quarry near the city of Barker (Figs. 1 and 3). Outcrops were mapped in detail and stratigraphic profiles constructed at centimeter resolution. High-resolution sampling further allowed for a comprehensive microfacies and diagenetic studies.

Petrography combined with X-ray diffraction (XRD) and scanning electron microscopic analysis (SEM-EDS) was performed to select the most suitable samples, which were microsampled to avoid surface weathering and recrystallized veins and fractures, for major, trace, and REE analysis by ICP-MS techniques. Polished thin sections of 30 samples were prepared and observed with a high-resolution petrographic microscope. Samples were stained

Table 2
Trace element contents (ppm) from samples of the Villa Mónica (CO) and Cerro Largo (PR and BK) formations.

Sample	Major elements (oxides %)										Trace elements (ppm)																	
	SiO_2	Al_2O_3	Fe_2O_3	CaO	MgO	Na_2O	K_2O	TiO_2	MnO	P_2O_5	Ba	Zr	Co	Cr	Cs	Cu	Ga	Hf	Nb	Ni	Pb	Rb	Sr	Th	U	V	W	Zn
CO.1	8.13	3.13	0.91	47.8	0.12	0.05	0.88	0.06	0.01	35.8	407	20	3.4	20	0.7	90	8.5	0.5	2.5	20	14	19.7	802	6.1	29.2	78	3	21
CO.2	19.05	8.64	1.15	37.7	0.33	0.08	2.62	0.3	0.01	28	445	79	3.2	20	1.8	48	14.6	2.1	9.5	22	19	50.2	477	4.1	39.1	87	2	26
CO.3	15.55	3.39	0.59	43.6	0.19	0.05	1.01	0.06	0.01	33.5	335	20	3.5	20	1.1	49	11	0.6	2.3	18	177	26	503	23.9	47	58	2	26
CO.4	19.7	2.92	0.67	41.4	0.13	0.06	0.83	0.06	0.01	30.9	1140	24	4.1	20	0.7	18	7.9	0.7	1.8	23	24	20.9	556	2.6	24.4	29	2	26
CO.5	12.2	5.11	76	1.12	0.69	0.11	1.34	0.2	0.02	0.17	388	28	1.2	<10	0.8	<5	6.9	0.5	1	<5	29	33.3	21	3.4	3.5	158	6	35
CO.6	53.9	5.97	20.1	6.18	0.81	0.04	0.86	0.78	0.21	1.24	3680	1090	74.5	70	2	470	14.2	25.8	21.6	125	17	17.4	140	12.5	13.1	94	10	164
COL 2B	17.15	3.38	0.53	43.6	0.17	0.05	0.93	0.07	0.02	30.8	1015	35	4.5	40	1.1	34	9.7	0.9	3.1	13	79	25.7	479	3	37.2	72	2	29
COL 5B	28.2	11.60	1.81	28.5	0.47	0.05	3.42	0.96	0.01	20.3	1065	167	5.8	150	4.5	43	20.0	3.4	29.1	21	22	81.1	335	12.3	32.4	236	2	41
PR.1	15.9	4.07	1.98	40.7	0.42	0.08	1.09	0.05	0.01	30.5	515	16	20.1	30	6.3	117	8.5	0.8	0.8	51	129	46.3	620	3.8	57.7	47	1	340
PR.2	23.3	2.18	2.18	39.6	0.39	0.04	0.38	0.03	0.01	29.4	542	9	11	30	4.1	13	3.9	0.3	0.6	20	36	17.4	597	0.9	6.21	22	1	114
PR.3	27.8	3.23	1.84	35.6	0.35	0.05	0.87	0.05	0.01	26.6	659	17	21.6	30	6.2	47	6.2	0.7	1	41	91	40	504	2.5	8.4	46	1	235
PR.4	13.95	1.64	0.66	45.9	0.15	0.08	0.48	0.02	0.02	32.3	365	9	4.8	20	1.4	15	5.8	0.7	0.4	9	58	19.7	653	1.1	13.5	17	1	107
PR.5	69	11.2	9.73	0.19	0.96	0.05	3.63	0.65	0.01	0.05	623	211	9.7	70	14.7	12	16.3	6.3	11.9	22	23	168.5	25.3	13.2	0.9	92	4	88
BK 1	14.1	2.92	1.4	44.1	0.31	0.05	0.79	0.05	0.02	30.3	728	58	3.9	20	0.9	14	5.8	1.7	0.9	12	6	29.2	556	3.9	10.1	36	1	107
POR −1B	20.6	4.49	2.12	39.9	0.42	0.09	1.21	0.06	0.01	27.9	409	26	18.7	50	7.7	100	10.5	1.2	1.3	51	94	58.7	691	7.3	33.7	69	2	284
CNPO −1	13.60	2.08	0.73	45.3	0.16	0.07	0.55	0.03	0.01	31.5	375	24	6.1	40	1.8	18	6.9	1.1	0.8	20	42	24.6	790	4.6	13.5	23	5	82

Table 3
RRE (PAAS normalized) concentrations, estimated ratios and anomalies; additional C and O isotope results for some samples.

Sample	La	Ce	Pr	Nd	Sm	Eu	Gd	Tb	Dy	Ho	Er	Tm	Yb	Lu	Y	Ce/Ce*	Ce anom	Ce/La	La/Sm	Pr/Pr*	Y/Y*	Eu/Eu*	Dy/Sm	Er/Lu	La/Nd	$\delta^{13}C$	$\delta^{18}O$	$^{87}Sr/^{86}Sr$
CO.1	101	231	28.9	126	29.7	9.6	36	5.2	29	5.3	14	1.7	9.8	1.4	212	0.971	−0.0127	2299	0.492	0.991	1378	1379	1138	9789	0.801			
CO.2	54.7	162	28.3	157	57.4	19	83	12	59	9.6	21	2.2	11	1.4	307	0.815	−0.0891	2962	0.138	0.962	1017	1303	1227	15.18	0.348			
CO.3	128	355	55	252	60.5	13	59	8.3	42	7.1	18	2	10	1.4	254	0.948	−0.0231	2784	0.306	1047	1166	1011	0.823	12.91	0.506	0.20	−11.29	
CO.4	85.4	205	31.4	151	42.6	13	54	8.1	44	7.9	20	2.4	13	1.8	320	0.866	−0.0627	2.4	0.291	1012	1.37	1253	1219	11.15	0.566			
CO.5	7.1	18	1.51	6.2	1.4	0.4	2	0.2	1.6	0.3	1	0.1	0.5	0.1	9.5	1189	0.07525	2465	0.737	0.849	1103	1115	1.33	7	1145			
CO.6	32.8	105	12.4	63	19	5.1	27	4	22	3.7	9	1.1	6.8	1	107	1099	0.04089	3186	0.251	0.88	0.951	1059	1358	9131	0.518	−1.42	−9.91	
COL2B	89.8	167	20	81	18.3	4.6	23	3	18	3.6	10	1.1	6.6	0.9	178	0.884	−0.0533	1854	0.715	1007	1746	1055	1189	10.43	1106			
COL5B	79.4	139	17.1	72	19.8	6.9	38	4.6	25	4.2	10	1.1	6.3	0.8	178	0.831	−0.0806	1744	0.585	0.999	1391	1194	1483	12.35	1103	−2.23	−5.68	
COLD1	Stromatolitic dolostone (base)																									−1.67	−3.86	0.70685
COLD25	Dolostone (top)																									0.95	−4.56	0.70706
PR.1	235	410	71.6	321	75.2	17	84	12	67	13	33	4	24	3.5	477	0.71	−0.1489	1745	0.454	1109	1303	1004	1.06	9.57	0.732	0.47	−11.06	
PR.2	59.9	91	14.8	61	13	3.6	15	2.3	13	2.6	7	0.9	6.2	0.9	115	0.697	−0.1567	1526	0.672	1135	1596	1198	1172	7839	0.979			
PR.3	147	220	37.8	166	38	9.2	43	6.1	34	6.6	18	2.2	14	2	270	0.66	−0.1806	1502	0.56	1118	1446	1072	1045	9179	0.883	−1.02	−11.64	
PR.4	197	376	72.6	376	98.8	25	122	17	91	17	43	4.7	27	3.9	685	0.662	−0.1791	1909	0.29	1.04	1383	1051	1095	11.04	0.524			
PR.5	42.4	67	7.91	24	3.05	0.6	2.9	0.4	2.1	0.5	2	0.3	1.9	0.3	13	0.864	−0.0634	1585	2.02	1152	1022	0.865	0.817	5536	1759			
BK 1	75.2	99	13.1	51	9.76	2.3	12	1.8	10	2.3	7	0.9	5.6	0.8	99	0.685	−0.1645	1314	1119	1078	1645	1011	1239	7927	1477			
POR1B	280	505	88.9	388	98.6	21	109	14	81	14	34	3.9	23	3.1	592	0.729	−0.1372	1804	0.413	1132	1398	0.97	0.979	10.92	0.722			
CNPO1	265	508	96.1	492	132	31	154	22	120	21	53	6.1	35	5.3	953	0.674	−0.1711	1917	0.292	1042	1504	1019	1074	9887	0.539			

with alizarin red S to differentiate between calcite and dolomite (Dickson, 1966). Twenty of the samples from three localities of the Villa Mónica and Cerro Negro formations were selected for whole rock and clay mineral (<2 μm fraction) analysis by XRD (Table 1).

These samples were ground with a rubber mortar, and repeatedly washed with distilled water to deflocculate the fine-grained clay minerals (Moore and Reynolds, 1989). The <2 μm fraction was separated by gravity settling, and oriented mounts were prepared on glass slides. Clay mineralogy was determined from diffraction patterns obtained using samples that were air-dried, ethylene glycol-solvated and heated to 550 °C for 2 h (Brindley and Brown, 1980). Diffractograms were run on a PANalytical model X'Pert PRO diffractometer (Centro de Investigaciones Geológicas, La Plata, Argentina) using Cu/Ni radiation at 40 kV and 40 mA. Routine air-dried mounts were run between 2° and 32° 2θ at a scan speed of 2° 2θ/min. Ethylene glycol-solvated and heated samples were run from 2° to 27° 2θ and 3° to 15° 2θ, respectively, at a scan speed of 2° 2θ/min. Semi-quantitative estimates of the relative concentrations of the clay minerals were based on the peak area method (Biscaye, 1965) on glycolated samples (001 for illite, smectite, kaolinite, pyrophyllite and mixed layer illite/smectite, and 002 for chlorite). Relative percentages of each clay mineral were determined by applying empirical factors (Moore and Reynolds, 1989). Semi-quantification was considered sufficient to define the clay mineral composition because presence/absence or dominant/subordinate relationships clearly allowed for the establishment of significant groups. All minerals present in the samples with abundances above 1% are reported (Table 1).

Selected samples were examined by scanning electron microscopy (SEM) using a Jeol 5900LV microscope (Facultad de Ciencias, Montevideo, Uruguay). Chips of samples were coated with Au and their elemental compositions determined by X-ray energy dispersive spectroscopy EDS (Thermo Scientific, UltraDry Silicon Drift Detector using the NORAN System 7 X-ray Microanalysis System for processing).

Sixteen phosphate samples, eight from the Villa Mónica Formation and the other eight from the Cerro Negro Formation, were selected for geochemical analyses of major, trace and rare earth elements, and five of these were also chosen for carbon, oxygen, and strontium isotope analysis (Tables 2 and 3). These samples were obtained from phosphate concretions and lenses, chert phosphate breccias, phosphate clasts, phosphatic and ferruginous shales. The samples from the Villa Mónica Formation correspond to CO1 to CO4 (phosphate concretions), CO5 (iron-rich shale) and CO6 (iron concretions), whereas COL2-B and COL5-B are phosphate lenses. On the other hand, the samples of the Cerro Negro Formation are phosphate concretions, with the exception of PR5, which is a matrix shale. Sample were carefully chipped to remove weathered surfaces, and subsequently cleaned and dried at 80 °C for two days. Subsequently, samples were crushed in an agate ball mill to obtain 230-mesh whole-rock powder, and analyzed for major, minor, trace and REE element concentrations by inductively coupled plasma mass spectrometry (ICP-MS), and by inductively coupled plasma atomic emission spectroscopy (ICP-ALS) using (loss on ignition at 1000 °C) WST-SEQ techniques at the ALS Minerals Laboratories.

Cerium anomalies were calculated as log $(3Ce_N/2La_N + Nd_N)$ (Elderfield and Graves, 1982), and the Eu anomaly was calculated as $Eu_N/(Sm.Gd)^{0.5}$ (McLennan, 1989). In addition, the Ce/Ce* represent $3Ce_N/(2La_N + Nd_N)$ while the Ce anomaly is the log of Ce/Ce*. Y/Y* was obtained from $2Y_N/(Dy_N + Ho_N)$, and Pr/Pr* from $2Pr_N/(Ce_N + Nd_N)$, where N refers to the normalization of concentrations against the standard post-Archean Australian Shale (McLennan, 1989).

Carbonate carbon and oxygen isotopes were measured rapidly by continuous flow-isotope ratio mass spectrometry in the University of Maryland Paleoclimate Co Laboratory using a refined method for the analysis and correction of carbon ($\delta^{13}C$) and oxygen ($\delta^{18}O$) isotopic composition of 100 μg carbonate samples (Spotl, 2011). Up to 180 samples loaded into 3.7 ml Labco Exetainer vials and sealed with Labco septa were flushed with 99.999% Helium and manually acidified at 60 °C. The carbon dioxide analyte gas was isolated via gas chromatography, and water was removed using a Nafion trap prior to admission into an Elementar Isoprime stable isotope mass spectrometer fitted with a continuous flow interface. Data were corrected via automated Matlab scripting on the Vienna PeeDee Belemnite and LSVEC Lithium Carbonate (VPDB-LSVEC) scale (Coplen et al., 2006) using periodic in-run measurement of international reference carbonate materials and/or in-house standard carbonates, from which empirical corrections for signal amplitude, sequential drift, and one or two-point mean corrections were applied. Precision for both isotopes is routinely better than 0.1‰. Including acidification, flush fill, reaction and analysis, true throughput exclusive of correcting standards is 2–3 samples/h, or up to 144 samples over a 40-h analytical session.

For analysis of strontium isotopic composition simple powders (ca. 5–10 mg) were leached three times in 0.2 M ammonium acetate (pH ~8.2) to remove exchangeable Sr from non-carbonate minerals, and then rinsed three times with Milli-Q water. The leached powder was centrifuged, decanted, and acidified with doubly distilled 0.5 M acetic acid overnight to remove strontium from the carbonate crystal structure. The supernatant was centrifuged to remove insoluble residues and then decanted, dried, and subsequently dissolved in 200 μl of 3 M HNO_3. Strontium separation by cation exchange was carried out using a small polyethylene column containing ~1 cm of Eichrom®Sr specific resin. The column was rinsed with 400 μl of 3 M HNO_3 before the dissolved sample was loaded onto the column. After loading, the sample was sequentially eluted with 200 μl of 3 M HNO_3, 600 μl of 7 M HNO_3, and 100 μl of 3 M HNO_3 to remove the Ca, Rb and REE fractions; the Sr fraction adsorbs strongly to the resin in an acidic environment. The Sr fraction was removed by elution with ~800 μl of 0.05 M HNO_3 and the resultant eluate collected and dried. Approximately 200–300 ng of the dried sample was transferred onto a degassed and pre-baked (~4.2 A under high vacuum) high purity Re filament with 0.7 μl of Ta_2O_5 activator. The prepared filaments were measured using the VG Sector 54 thermal ionization mass spectrometer in the TIMS facility of the University of Maryland Geochemistry Laboratories. Filaments were transferred to a sample carousel, heated under vacuum ($\sim10^{-7}$–10^{-8} atm) to a temperature between 1450 and 1650 °C, and analyzed when a stable signal (>1.0 V) was detected on the mass 88 ion beam. Approximately 100 $^{87}Sr/^{86}Sr$ ratios were collected for each sample. Final data have been corrected for fractionation using the standard value $^{86}Sr/^{88}Sr = 0.1194$. The fraction of ^{87}Sr resulting from in situ decay from ^{87}Rb was removed by measurement of rubidium abundance at mass 85. Repeated analysis of the NBS SRM987 standard yields an average value of $^{87}Sr/^{86}Sr = 0.71024448 \pm 0.0000111$ (2σ) during the analytical window.

4. Results

4.1. X-ray diffraction

4.1.1. Villa Mónica Formation

The concretionary phosphate samples contain abundant quartz, with variable amounts of feldspar, fluorapatite (in phosphatic concretions and lenses) and clay minerals (Fig. 4a). Dolomite is abundant in two samples of edgewise conglomerate in which the carbonate mineral constitutes the majority of matrix material. Calcite is present in five samples in varying abundances, and goethite is present in one sample from an iron-rich concretionary level (Table 1). Clay minerals (<2 μm) are dominated by illite (60–90%),

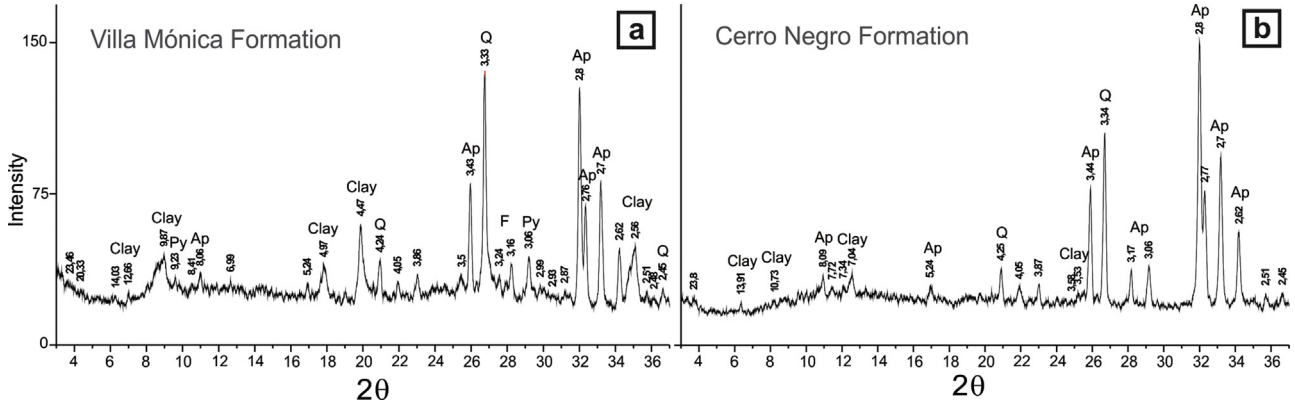

Fig. 4. X-ray diffractograms from bulk rock analysis of phosphatic levels from the Villa Mónica (a) and Cerro Negro (b) formations. References: Py: pyrophyllite, Ap: apatite, Q: quartz, F: feldspar.

with lesser amounts of mixed-layered illite–smectite (10–20%), chlorite (0–20%), mixed-layered chlorite–smectite (0–8%), kaolinite (0–15%), and smectite (0–5%). Pyrophylite is rare and was only clearly identified in one sample (Table 1). The crystallinity index of illite (IC; Kubler, 1967) varies from 0.4 to 0.6, which is suggests a diagenetic origin for this mineral, while an Esquevin index (IE; Esquevin, 1969) of 0.25–0.36 suggested an intermediate ferromagnesian to aluminous composition for these samples (Table 1).

4.1.2. Cerro Negro Formation

The composition of phosphate concretions from the Cerro Negro Formation include moderate to very abundant quartz, with only traces of feldspar and clay minerals. Calcite was either absent or very abundant. Fluorapatite was scarce to very abundant in samples of concretionary levels and absent in samples of the mudstone matrix (Fig. 4b). No iron-bearing minerals were identified in samples from this formation (Table 1). The clay fraction indicated a preponderance of illite (70–90%), scarce to absent illite–smectite mixed layer (0–10%), traces to scarce chlorite (tr–10%), and absent to scarce chlorite–smectite mixed layer (0–15%). Kaolinite was identified only in one sample at around 10% of the clay fraction. The illite crystallinity index of samples was generally around 0.45, indicating a probable diagenetic origin due to the transformation from smectite, and the Esquevin index is near 0.4, suggesting a ferromagnesian affinity (Table 1).

4.2. Petrography and SEM

4.2.1. Villa Mónica Formation

Centimeters below the phosphate level, a laminated gravelly mudstone was previously described and petrographically characterized (Poiré, 1989; Gómez-Peral et al., 2011; Fig. 5a and b). Our current petrographic analysis makes it possible to distinguish three phosphatic microfacies (MP1, MP2 and MP3; Fig. 5). MP1 is composed of microcrystalline and cryptocrystalline fluorapatite, which constitutes the main mineralogical phase of the concretions. MP2 is characterized by micro- and cryptocrystalline fluorapatite with spherulitic microstructure; surrounding these spherulites (20–30 μm in diameter) the most common cement is chert, but some irregular microfractures filled by hematite and goethite are also present (Fig. 5c and d). The third microfacies, MP3, is represented by concretions that are internally composed of mono- and polycrystalline quartz (with sand size ranging from 200 μm to 1 mm) floating in a phosphate cement with isotropic extinction (Fig. 5e).

Phosphate clasts (from the base of the dolomitic facies association) are well rounded and compositionally identical to the concretions described above (Fig. 5f). These clasts are cemented by (a) iron-rich dolosparite with idiotopic texture and crystals about 150 μm in size; (b) dolomicrite, dolomicrosparite and fine-grained dolosparite (~4–30 μm) with hypidiotopic and xenotopic texture; (c) reddish ferruginous cement; (d) chert as replacement of dolomite and (e) calcite in veins and also as dedolomitization replacement (Fig. 5f). In the Piedra Amarilla Quarry, phosphate clasts in the fill of the intersteses between columnar stromatolites and are associated with subrounded to rounded quartz and mudstone intraclasts. SEM observations show that the phosphates show hexagonal or pseudocubic euhedral microcrystals of about 2 μm in size (Fig. 5g and h). Clay, occurring as cracked cements coating mineral grains, has also been identified (Fig. 5e and f). EDS analyses indicates that the phosphates have high contents of P, Ca and C, as expected for mixtures of apatite and calcite.

4.2.2. Cerro Negro Formation

Petrographically, phosphate concretions in the Cerro Negro Formation are composed almost entirely by crypto- to microcrystalline fluorapatite with associated chert and residual clays. Fractures in the concretions are sometimes filled with ferroan calcite cement and iron oxides (Fig. 6a and b). SEM-EDS analysis makes it possible to recognize subhedral to anhedral fluorapatite crystals that are commonly of <1 μm in diameter (Fig. 6c and d). EDS analyses show that the samples are primarily composed of francolite, but chert and other minor silicates are also recognized.

4.3. Major and trace elements

Chemical analyses show variable P_2O_5 contents in the phosphate samples, ranging from 20 to 36% in those from both the Villa Mónica and Cerro Negro formations. In the Villa Mónica Formation, the phosphate concretions are associated with ferruginous shale (containing 20% Fe_2O_3) including iron-rich concretions with up to 76% Fe_2O_3 (Table 2). The iron minerals were identified by X-ray diffraction as goethite (4.18 Å) and hematite (2.69 Å). In the Cerro Negro Formation, phosphate is concentrated in shale and marl (as matrix minerals), and in cherty concretions that have low iron contents ($Fe \leq 2.2\%$). Phosphorous in both the Villa Mónica and Cerro Negro samples is also associated with high concentrations of CaO (30–48%), as expected for francolite (Table 2). The shale matrix (sample CO6) from the Villa Mónica Formation has relatively higher proportions of Ba (3680 ppm), Zr (1090 ppm), Cu (470 ppm), Co (70 ppm), Ni (150 ppm) and Zn (164 ppm) than the concretions (Table 2). Of the samples from the Cerro Negro Formation, PR5 (the shale matrix) contains elevated Zr (211 ppm) relative to the concretions. Phosphate samples of this unit are characterized by

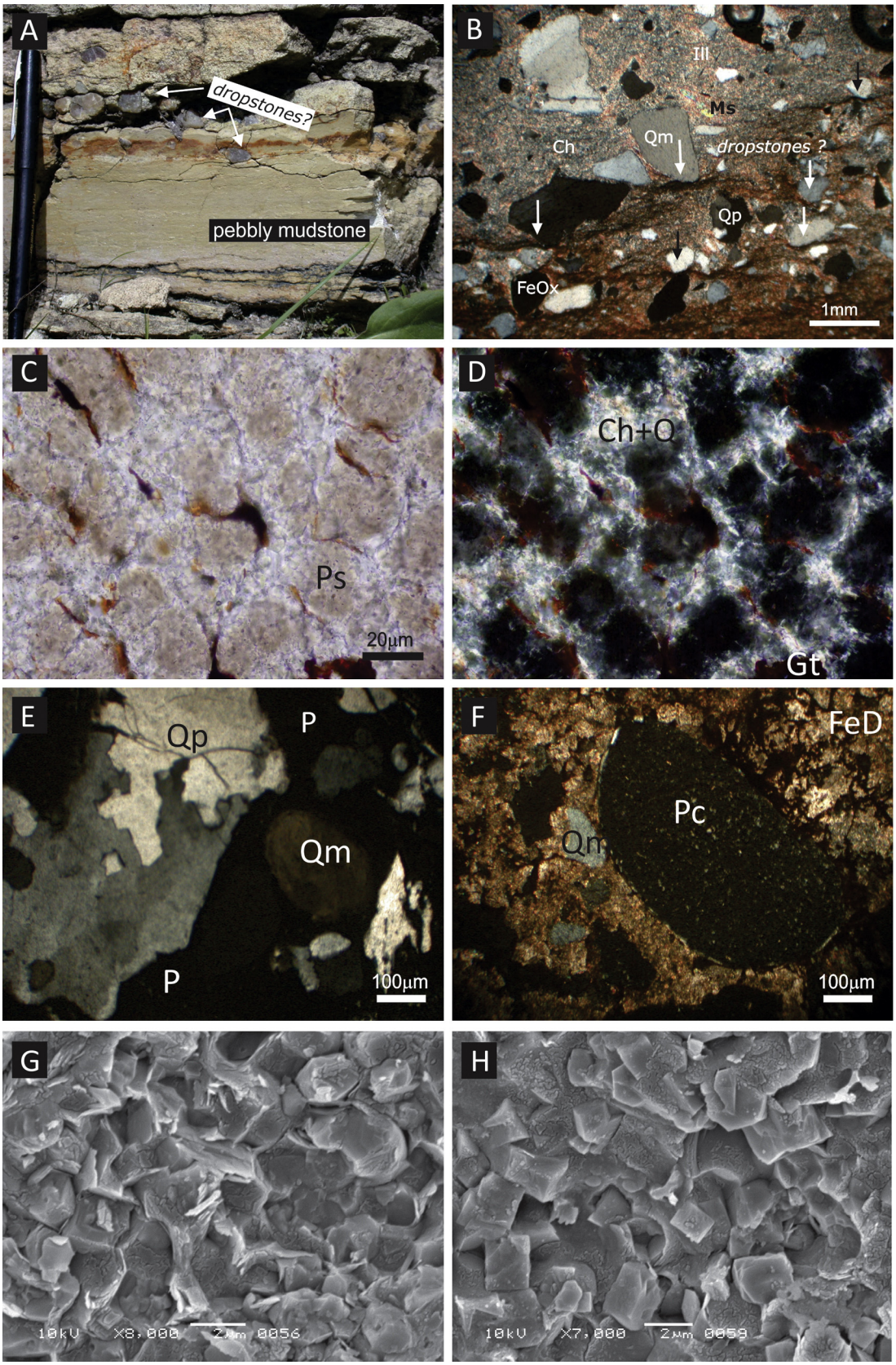

Fig. 5. Petrographic and SEM microphotographs from the VMF phosphate level. (A) and (B) Laminated mudstone with dropstones (modified from Gómez-Peral et al., 2011); (C) and (D) Spherulitic texture of francolite (MP1) without and with crossed nicols. (E) Quartz grains rounded by phosphatic cement. (F) Rounded phosphatic clast in dolomitic cements. (G) and (H) SEM photos showing fluorapatite crystals (P) with hexagonal and pseudocubic habits (see text for brief explanation).

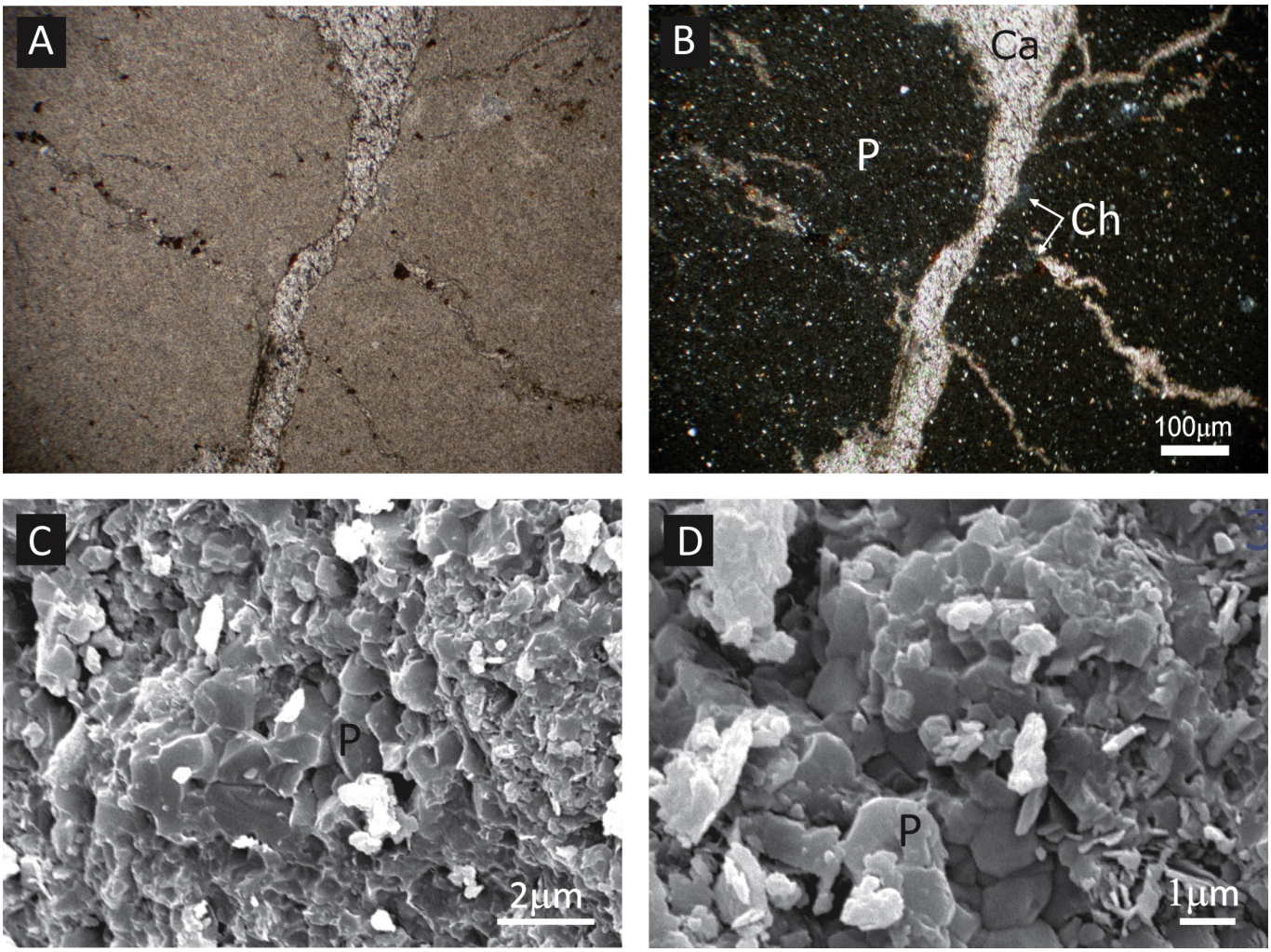

Fig. 6. Petrographic and SEM microphotographs from upper CNF phosphate level. (A) and (B) Cryptocrystalline fluorapatite (P) of the inner concretions. (C) and (D) SEM photos showing in detail the anhedral to subhedral francolite crystals (P).

average concentrations of Ba (527 ppm), Zr (23 ppm), Cu (42 ppm), Co (13 ppm), Ni (28 ppm), Zn (181 ppm) (Table 2).

4.4. REE abundances

If well preserved, the distribution patterns of the REEs in sedimentary apatite can be similar to those in co-eval sea water or marine pore fluids (German and Elderfield, 1990; Jarvis et al., 1994; Bertrand-Sarfati et al., 1997; Shields and Stille, 2001; Hannigan and Sholkovitz, 2001; Picard et al., 2002; Chen et al., 2003). Modern oxidized seawater is characterized by having progressively greater abundance of REEs with a notable depletion of Ce enrichment of Eu relative to adjacent elements (Bau and Dulski, 1996). Total REE contents in the Villa Mónica phosphate concretions range from 311 to 1010 ppm (596 ppm on average), while those in the Cerro Negro phosphorites vary from 290 to 1470 ppm (760 ppm on average); as expected REE concentrations are lower in the mudstones and shales associated with these concretions (40 and 155 ppm, respectively). PAAS-normalized REE concentrations (Taylor and McLennan, 1985; McLennan, 1989) were plotted for the two formations on a log-scale diagram (Fig. 7). All values are similar or slightly higher than the averages reported for ancient bedded phosphorites (Altschuler, 1980; Kolodny, 1981; Kolodny and Luz, 1992; Ilyin, 1998). We observe LREE and HREE (Ilyin, 1998; Mazumdar et al., 1999) depletions relave to MREEs in both of the studied units (Table 3; Fig. 7), which likely reflect elemental redistribution associated with the formation of francolite. Yttrium, in particular, is highly enriched in the phosphorite samples of the Villa Mónica and Cerro Negro formations, varying from 107 to 320 and from 99 to 952 ppm, respectively. These concentrations are comparable with the global average for ancient phosphorites (ranging from 40 to 610 ppm; Altschuler, 1980; Mazumdar et al., 1999) (Table 3). Ce/La varies from 1.8 to 3.0 in the Villa Mónica concretions, but is lower in those from the Cerro Negro Formation, which vary between 1.3 and 1.9. The Ce/La of modern sea water (ranging from 0.2 to 0.3) and of ancient shale (typically ranging from 2 to 3) are believed to influence Ce/La in phosphorites in proportion to their respective contributions to the phosphorites (O'Brien and Veeh, 1983), which is consistent with our data. The presence of sporadically disseminated veins of barite in dolostone samples of the Villa Mónica Formation was recognized by SEM-EDS analysis and, in the shale sample of this unit a high Ba concentration of 3700 ppm was observed (Table 2). Eu concentrations vary between 5 and 19 ppm in the lower phosphorite horizon and from 2 to 30 ppm in the upper. Significantly lower concentrations of Eu were found in the shales and iron-rich concretions with <1 ppm in each.

4.5. Ce and Eu anomalies

Phosphorites formed under oxygenated conditions tend to have elevated REEs and negative Ce anomalies. In contrast, those

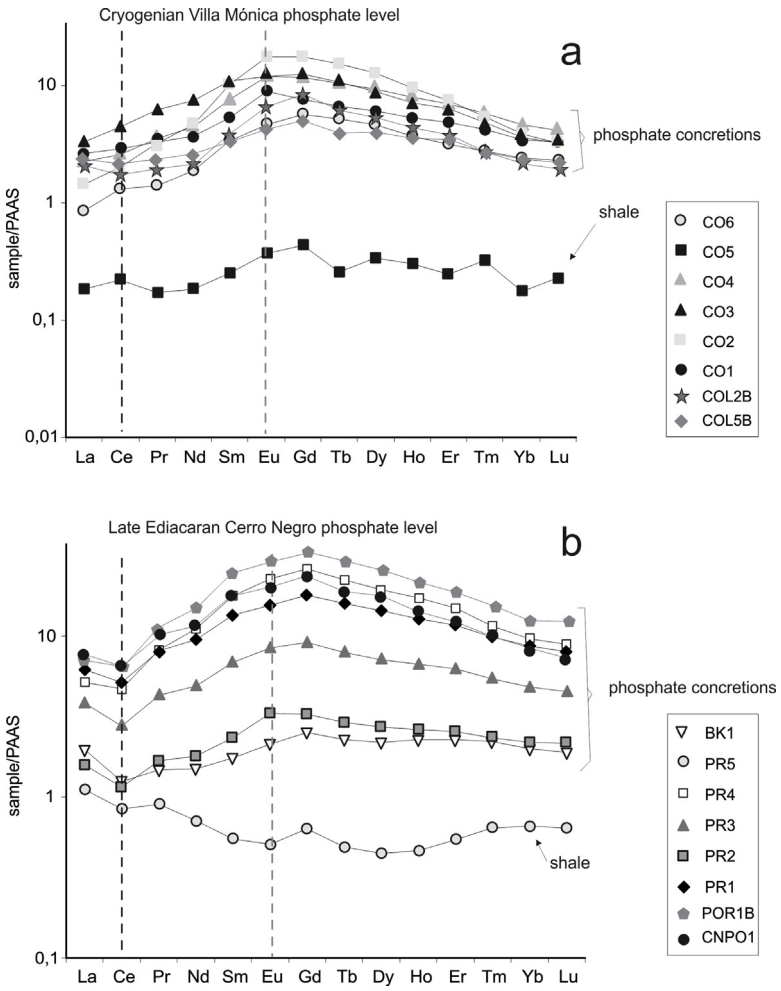

Fig. 7. PAAS-normalized REE distribution of the phosphate concretions from the two levels of the Tandilia System. (a) Villa Mónica Formation samples. (b) Cerro Negro Formation samples.

forming under more reduced conditions reveal little evidence for Ce enrichments relative to adjacent REEs, but do show positive Eu anomalies (Holser, 1997; Jarvis et al., 1994; Laenen et al., 1997; Ilyin, 1998). These anomalies result from the solubility of Ce and Eu bearing species in seawater relative to their oxidation state (Sholkovitz et al., 1994). For example, if oxidizing conditions are encountered, Ce^{3+} will oxidize to Ce^{4+} and become insoluble thus depleting the element in the water column; if francolite is subsequently formed from solution, the negative Ce anomaly would be inhereted (McArthur and Walsh, 1984). Thus, Ce anomalies (related to other REE) have been used to infer paleo-oceanic redox conditions (Wright et al., 1987; Liu et al., 1988; Bertram et al., 1992; Jarvis et al., 1994; Holser, 1997; Yang et al., 1999; Mazumdar et al., 1999; Shields and Stille, 2001; Xiao et al., 2012). One of the more important considerations often overlooked is the fact that the oxidation state of Ce may be more sensitive to pH than to PO_2.

Wright et al. (1987) defined Ce anomalies of <−0.1 as indicative of oxidizing conditions (heretofore described as a negative anomaly) and Ce anom >−0.1 (heretofore described as a positive anomaly) as indicating anoxic conditions. However, while *negative* Ce anomalies in apatite may be a strong redox indicator of the primary water body, *positive* anomalies are more likely to be diagnostic of suboxic to anoxic diagenetic conditions (Holser, 1997; Laenen et al., 1997). Many ancient phosphorites are known to record negative Ce anomalies (Jarvis et al., 1994; Ilyin, 1998; Mazumdar et al., 1999; Morad and Felitsyn, 2001; Chen et al., 2003). In our data set both the Villa Mónica and the Cerro Negro phosphate concretions record Ce anomalies ranging from −0.09 to +0.08 and from −0.18 to −0.06, respectively (Table 3, Fig. 7). Applying the constraints suggested by Wright et al. (1987), the former would indicate an anoxic environment while the latter would be oxidized.

Most of the paleo-oceanic models presented for the Neoproterozoic (Holser, 1997; Donnelly et al., 1990; Brasier, 1992; Logan et al., 1995; Kimura et al., 1997; Mazumdar et al., 1999; Canfield et al., 2008) suggest significant variations in the redox architecture of ocean margins. In all these models, an oxygen-depleted deep ocean lies below oxygenated surface water, but in some cases there may be locally enhanced euxinic conditions (free H_2S in the water column) either localized in lagoonal settings behind rimmed margins (Jiang et al., 2011) or in a wedge-shaped geometry on ramps (Li et al., 2010). Marked thermohaline stratification and diminished vertical circulation during the Neoproterozoic (Brasier, 1992; Mazumdar et al., 1999) may have enhanced redox stratification of shallow oceans, which are potentially recorded as negative $\delta^{13}C$ values in carbonates and co-existing organic carbon (Aharon et al., 1987; Banerjee et al., 1997; Mazumdar et al., 1999). Cook and Shergold (1986) suggested that phosphorite development is related to the upwelling of deep anoxic ocean water onto shallow oxygenated shelves. Mixing of the two water masses would thus transfer phosphorous and Ce from the deep environment to shallow environments where the elements would be sequestered into sediments by enhancing primary productivity.

However, the magnitude and sign of Ce anomalies may be modified by later diagenetic concentration of the REE in apatite

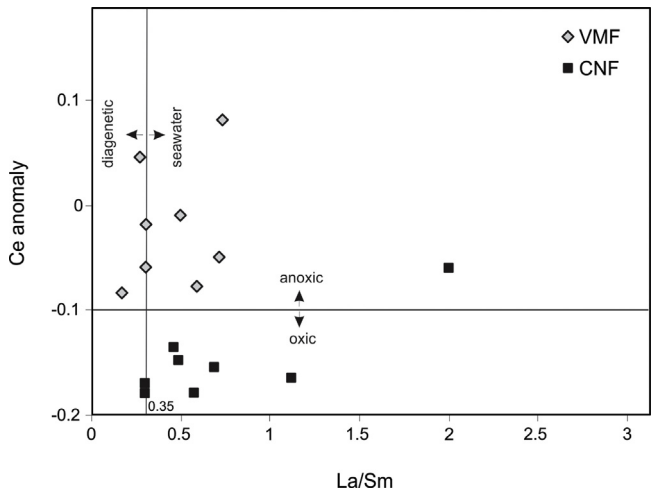

Fig. 8. Crossplot of Ce anomaly vs. La_N/Sm_N plotting the ratios of samples of the Villa Mónica and Cerro Negro formations (VMF and CNF).

(McArthur and Walsh, 1984; Shields and Stille, 2001; Morad and Felitsyn, 2001) so that depositional values are reset toward more positive numbers. Confidence that our positive Ce anomalies are not reset thus requires independent evidence. These researchers have suggested that Ce anomalies in apatite represent depositional conditions only if the anomaly does not correlate with La_N/Sm_N, and that La_N/Sm_N are >0.35. In this respect, some of the samples from the Villa Mónica Formation and most of those from the Cerro Negro Formation fulfill this requirement (Table 3; Fig. 8). Shields and Stille (2001) further show that later diagenetic processes result in (1) the positive correlation of Ce and Eu anomalies, (2) the negative correlation between Ce anomaly and Dy_N/Sm_N, and (3) a positive correlation between Ce anomaly and total REE abundances in phosphorites. We do not recognize these relationships in our samples from the Tandilia phosphorites (Fig. 9), supporting the view that diagenetic alteration of the REE patterns and Ce and Eu anomalies were limited. For these reasons, we conclude that the Villa Mónica and Cerro Negro phosphorites likely reflect paleoseawater redox conditions (Fig. 9c).

As indicated above, samples from the Villa Mónica Formation reveal positive Ce anomalies, suggesting suboxic to anoxic conditions. In the same samples positive Eu anomalies (ranging from 1.05 to 1.75 in phosphorites and 1.11 in the iron-rich concretion; Table 3, Fig. 7a) are found. Conversely, in all of the Cerro Negro phosphate concretions, Ce anomalies are strongly negative (Fig. 7b), indicating oxidized conditions, and no Eu anomalies are revealed (Table 3, Fig. 6b). Some authors (Bau and Dulski, 1996; Shields and Stille, 2001; Chen et al., 2003) suggest that negative Ce anomalies may be overestimated if La is enriched by diagenetic processes. Considering the La concentrations in our samples, we find that Ce anomalies in four samples of the Villa Mónica Formation and in all samples of the Cerro Negro Formation are likely to be depositional, but that for the other samples the anomaly may be diagenetic in origin (Fig. 8).

According to different authors (Bau and Dulski, 1996; Shields and Stille, 2001; Chen et al., 2003), the negative Ce anomaly may be overestimated if La is enriched related to PrN or NdN. We find that Ce anomalies in two samples of the Villa Mónica Formation are really positive, while six samples of the Cerro Negro Formation display real negative Ce anomalies (Fig. 10). The absence of Ce anomalies in the rest of the samples could be explained as the result of LaN enrichment.

Interestingly, both the iron-rich concretion and the ferruginous shale from the Villa Mónica Formation show positive Ce anomalies (Table 3; Fig. 10). If primary, these observations may indicate that seawater (or pore fluids) was both anoxic and rich in iron. Alternatively, the negative Ce anomalies of phosphate concretions in the Cerro Negro Formation may suggest oxic seawater conditions on a well mixed and ventilated shallow water platform (i.e., marls, sandstone-limestones). This result is important insofar as the underlying sediments of the Loma Negra Formation preserve evidence for *Cloudina*, the quintessential Ediacaran biomineralized organism, which likely required oxygen for its metabolic activities (Gaucher et al., 2005).

Positive Eu anomalies are rarely recorded in marine sediments due to immobile nature of this element with respect to both depositional and slightly diagenetic environments. Nonetheless, positive anomalies have been recorded in BIF, chert and other chemical sediments (e.g., Stern et al., 2013) and these have been interpreted to reflect oceanographic conditions. In some cases, Eu anomalies may be correlated with high contents of Ba and be considered as indicative of high productivity (Mazumdar et al., 1999). Most of the Villa Mónica phosphate concretions reveal positive Eu anomalies and only slightly negative Ce anomalies, suggesting reducing conditions. We believe these reflect depositional conditions in the deeper ocean, with the likelihood that overlying shallow seawater may have been more oxidized, resulting in a gradient or stratification with respect to oxygen (see Canfield et al., 2008; Frei et al., 2013). On the other hand, Cerro Negro phosphate concretions reveal no Eu anomalies, which coupled with strong negative Ce anomalies, is in agreement with oxic conditions during the latest Ediacaran Period in this basin (Fig. 11; Mazumdar et al., 1999). Comparative studies are required to evaluate whether the signal is global or whether there may have been variations in the redox architecture of different basins at this time.

4.6. Stable isotopes (carbon, oxygen, and strontium)

Time-series carbon and oxygen isotope analyses of carbonates in the Sierras Bayas Group reveal evidence for both temporal variations and diagenetic overprints (Gómez-Peral et al., 2007; Bagnoud-Velásquez et al., 2013; Fig. 3). In the basal dolostone facies of the Villa Mónica Formation, a negative-to-positive $\delta^{13}C$ excursion of up to 4.5‰ was previously recognized (Fig. 3), which was interpreted as being related to a post-glacial accumulation of cap carbonate (Gómez-Peral et al., 2007, 2012; Bagnoud-Velásquez et al., 2013). Underlying the dolostones, a discrete level (less than 3 m) of laminated mudstones with potential dropstones was recently observed (Gómez-Peral et al., 2011; Figs. 3 and 5a and b). If substantiated, this sedimentologic observation might support a Cryogenian age assignment for this part of the succession.

On the other hand, the top of the upper carbonate succession, the Loma Negra Formation, is truncated by a karstic surface over which the phosphate nodules were developed (Fig. 3). Time-series measurements of the argillaceous carbonates in the Loma Negra Formation revealed consistently positive $\delta^{13}C$ values (ranging between +3 and +4‰; Fig. 3), which have been considered as reflecting depositional conditions (Gómez-Peral et al., 2007). Notably, $\delta^{18}O$ values fall from −7 to −14‰ toward the middle of the unit and from −14‰ to −9‰ top of the sequence (Gómez-Peral et al., 2007), which are represented in all sections studied. Poiré et al. (2007) and Gómez-Peral et al. (2012) suggest that these too reflect primary signatures associated with a decrease in seawater temperature toward the top of the unit associated with progressive glaciation and sea level fall. In agreement to this interpretation, the transfer of water from the ocean to continental glaciers should result in the ^{18}O enrichment of seawater due to the distillation effect associated with evaporation. Furthermore, the decreasingly negative $\delta^{18}O$ values beneath a karstic unconformity might reflect the cooling of seawater.

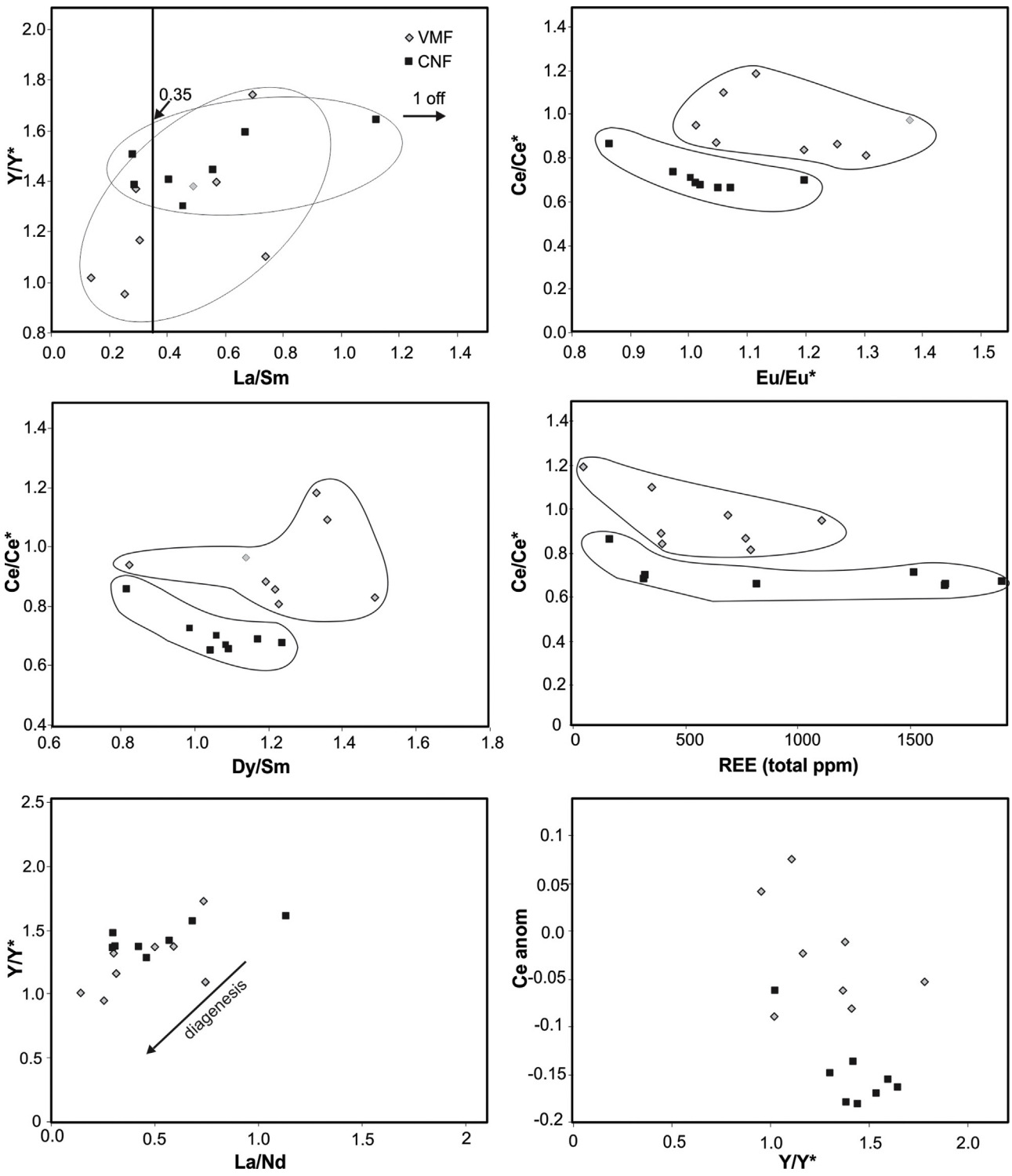

Fig. 9. Crossplots of some parameters involved in the study of the shale-normalized REE abundances of the phosphate concretions of both formations. Plots show there is no correlation between parameters of shale-normalized REE abundances.

The carbon and oxygen isotope results for the present study reveal that the $\delta^{13}C$ values of the Villa Mónica phosphorites range from −2.2 to 0.2‰ similar to other ancient phosphorites irrespective of age (Shemesh et al., 1988). Carbon isotopes are used to define phosphorite formation in the different oxic, suboxic and anoxic (sulfate reducing) environments in sea-floor sediments (Nathan and Nielsen, 1980; McArthur, 1985; Banerjee et al., 1986; McArthur et al., 1987; Compton et al., 1993; Sadaqah et al., 2007). The negative carbon isotopic composition of CO_3 in the francolite structure indicates that it likely formed within the oxic to suboxic zone (Fig. 11), perhaps associated with the anaerobic oxidation of organic matter (Fig. 3).

Two calcitic samples from the dominantly dolomitic Villa Monica Formation were analyzed for strontium isotope abundances (Table 3). These record $^{87}Sr/^{86}Sr$ values of 0.7069 and 0.7071, which are similar to those recorded in late Tonian or earliest Cryogenian

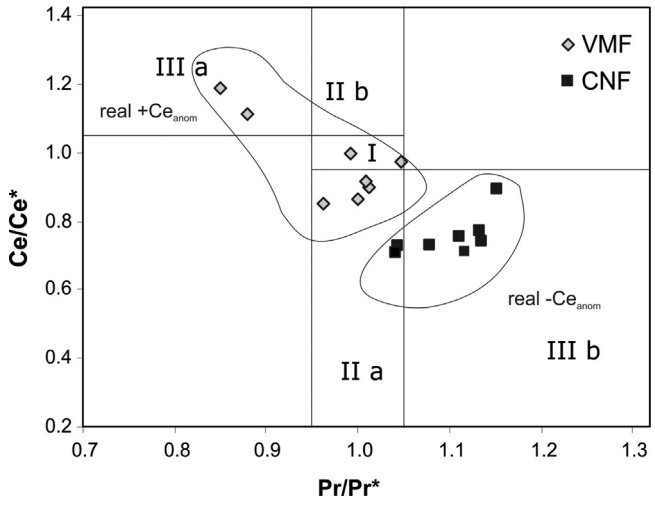

Fig. 10. Ce/Ce* vs. Pr/Pr* diagram after Bau and Dulski (1996). This plot evaluates the possible overestimation of negative Ce anomalies due to La enrichment in phosphorites of the Villa Mónica and Cerro Negro formations. Field I: no Ce anomaly and no La anomaly; Field IIa: positive La anomaly, no Ce anomaly; Field IIb: negative La anomaly, no Ce anomaly; Field IIIa: positive Ce anomaly; Field IIIb: negative Ce anomaly. In the phosphates of the Villa Mónica Formation (VMF) there are two samples with real positive Ce anomalies, while the others have false Ce anomalies. In the Cerro Negro Formation, most of the samples have true negative Ce anomalies with one exception.

limestones from Neoproterozoic successions elsewhere (Kaufman et al., 2009; Halverson et al., 2010). However, given that the process of dolomitization typically flushes strontium from calcitic or aragonitic sediments resulting in enrichment of strontium-87 (Jacobsen and Kaufman, 1999), these results provide only maximal constraints and should be interpreted with caution.

5. Diagenesis

Petrographic observations coupled to XRD and SEM analyses make it possible to evaluate the degree of incipient recrystallization from amorphous phosphate to cryptocrystalline francolite during diagenesis (Figs. 5 and 6). Spherulitc textures are considered here as primary in origin (Fig. 5a and b). REE concentrations, their distribution patterns, and presence or absence of Ce and Eu anomalies in marine sediments may also be useful indicators of post-depositional processes (Ilyin, 1998; Yang et al., 1999; Mazumdar et al., 1999; Chen et al., 2003). For that reason, it is important to emphasize that the highly variable REE patterns in phosphorites typically result from variations in detrital inputs, depositional environments, pore water redox conditions, pH, age and water depth (Bertrand-Sarfati et al., 1997; Chen et al., 2002; Nelson et al., 2010). In addition, REE signatures can be altered by burial diagenesis or by weathering (Shields and Stille, 2001; Chen et al., 2002; Baioumy, 2011).

The Er_N/Lu_N ratios of the Villa Mónica phosphorites range from 1.58 to 2.31, and the upper phosphorites of the Cerro Negro vary between 1.19 and 1.68 (Table 3). These ranges are consistent with ratios observed in late Ediacaran phosphorites (1.73–3.37) that appear not to have suffered diagenetic HREE exchange (Shields and Stille, 2001; Chen et al., 2003). The fact that HREE depletion is so commonly observed in well-preserved samples (Shields and Stille, 2001) also suggests that the ratios reflect synsedimentary conditions, rather than the by-product of later diagenesis. These authors suggest weathering should produce a positive correlation between La_N/Sm_N and Y/Y*. There is no correlation between these variables in the phosphates of the Tandilia System (Fig. 9a) suggesting that surficial or subsurface weathering of our samples is not a concern.

REE patterns can similarly be altered during deep burial and metamorphism (Elderfield and Pagett, 1986; Elderfield and Sholkovitz, 1987; German and Elderfield, 1990; Murray et al.,

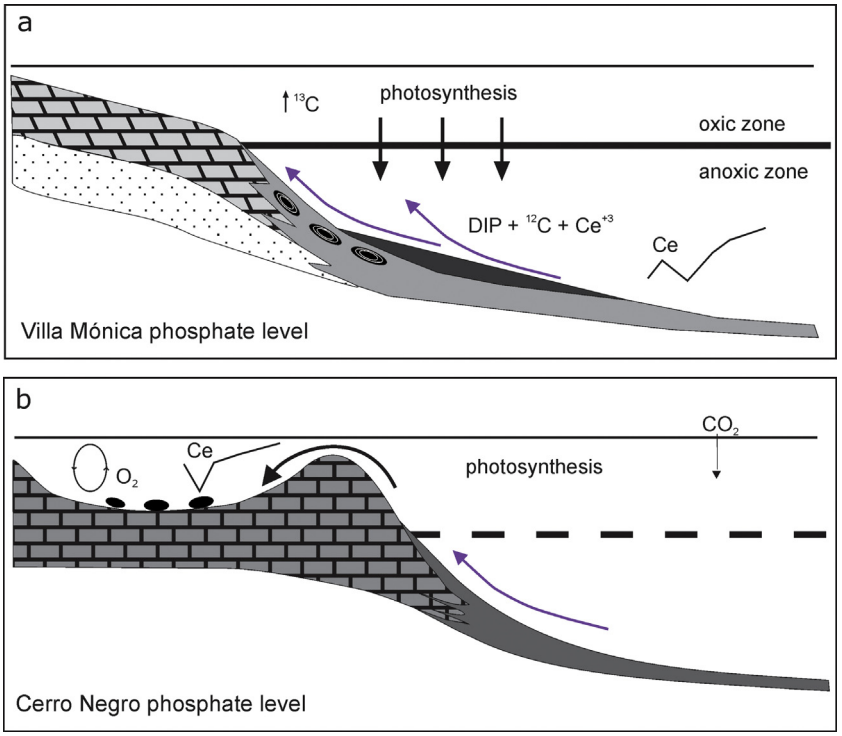

Fig. 11. Schematic representation to explain the genesis of dissolved inorganic phosphorus (DIP), ^{12}C and Ce enrichment in anoxic water below the redoxcline in a Neoproterozoic stratified ocean basin, modified from Mazumdar et al. (1999). (a) Paleoenvironment of the Villa Mónica Formation with a stratified basin where low Eh and pH conditions facilitate the reductive transformation of Ce^{4+} into soluble Ce^{3+}, giving a positive Ce anomaly. The redoxcline is a zone that separates the oxic and anoxic parts of the stratified sea basin. (b) Paleoenvironment scheme of the Cerro Negro Formation with well-mixed ocean and normal circulation of oxygen with negative Ce anomalies: organic matter (OM) is quickly remobilized by aerobic oxidation.

1992; Lécuyer et al., 1998; Reynard et al., 1999; Shields and Stille, 2001; Chen et al., 2003; Baioumy, 2011) potentially due to thermally induced transfer of REEs from clastic debris to phosphorites (McArthur and Walsh, 1984). Insofar as we do not observe obvious recrystallization of either carbonates or phosphates from the Sierras Bayas Group, it is unlikely that these rocks have experienced such metamorphic effects.

The shale-normalized REE patterns of these phosphate horizons are characterized by both LREE and HREE depletions relative to MREEs (Fig. 5), which is typical of ancient phosphorites. However, they are differentiated by the positive Ce and Eu anomalies in the lower horizon and negative Ce anomalies in the upper horizon. Based on our integrated petrographic, XRD, SEM, elemental and isotopic studies of these nodular phosphates, we conclude that most of the samples are well preserved and can be used as proxies for paleo-oceanographic conditions during their formation.

6. Discussion

The geochemistry of phosphorites and their constituent mineral francolite have been widely studied to estimate ancient seawater chemistry (Donnelly et al., 1990). The chemical composition of carbonate fluorapatite is highly variable because its crystal structure allows a variety of substitutions including REEs, sulfur and strontium. As mentioned above, REE signatures can be altered by burial diagenesis (Shields and Stille, 2001), or by surface weathering (Hannigan and Sholkovitz, 2001), so using the REE signatures of phosphorites to reconstruct paleoenvironments should be done with great caution. With this caveat in mind, our petrographic observations and geochemical analyses suggest that the Sierras Bayas phosphorites are well preserved and can be used as proxies of their depositional environment.

Phosphorite is a marine biochemical sedimentary rock generally associated with coastal upwelling (e.g., Glenn et al., 1994). In the Phanerozoic, this process governs primary productivity (Filippelli and Delaney, 1994), and ultimately controls the rate at which carbon dioxide is removed from the atmosphere and deposited as sedimentary organic matter (Föllmi et al., 1991). The accumulation of organic-rich (and phosphatic) strata is thus an important feedback that to some degree regulates climate.

In the Cerro Negro phosphate horizon, shale-normalized, seawater-type REE patterns characteristically show a progressive enrichment toward the heavier REEs and a relative depletion of Ce with respect to its REE neighbors La and Pr, or Nd. This negative Ce anomaly (Ce/Ce^*) is considered to be related to the decrease in solubility that accompanies the oxidation of Ce^{3+} to Ce^{4+} and their subsequent removal together with other multivalent metals (Sholkovitz et al., 1994). On the other hand, most surface water bodies are HREE enriched, but only those which contain free oxygen show a negative Ce anomaly. The Ce depletion in sea water does not solely depend on the oxidation potential (German and Ederfield, 1990), but also on microbial activity that catalyzes the oxidation of Ce^{3+} and controls the pH of pore fluids. Therefore, any Ce anomaly is likely to reflect the redox and pH conditions during deposition and, more importantly, those conditions may be preserved during diagenetic REE enrichment (Shields and Stille, 2001).

HREE depletion in phosphorites (Ilyn, 1998; Mazumdar et al., 1999; Shields and Stille, 2001; Chen et al., 2003) has been interpreted (1) to reflect the primary REE pattern of sea water (McArthur and Walsh, 1984; Ilyn, 1998; Mazumdar et al., 1999), (2) to record diagenetic modification (McArthur and Walsh, 1984; Mazumdar et al., 1999), and (3) to result from weathering processes (Shields and Stille, 2001). The Er_N/Lu_N ratios in our samples vary from 1.20 to 2.30, and these ranges are consistent with the same ratios of Cambrian phosphorites (1.73–3.37) that are believed not to have not suffered diagenetic HREE exchange (Shields and Stille, 2001; Chen et al., 2003).

6.1. Phosphogenesis and glaciation

Based on the stratigraphic context and our petrographic and geochemical observations of the phosphate horizons we explore here whether the development of phosphate was related to glacial eustacy in the Cryogenian and Ediacara intervals. This speculation follows Cook and Shergold's (1986, 2005) suggestion that periods of glaciation can produce a great volume of cold, nutrient-rich waters, resulting in a major expansion of organic productivity in the photic zone and development of phosphorite (Misi and Kyle, 1994).

Clear lithostratigraphic evidence for glaciation is lacking in the Sierras Bayas Group, although potential dropstones in laminated facies of the basal Villa Mónica Formation have been observed. The distribution and composition of these outsized clasts, and whether they preserve striations is unknown at present and requires further field observations. On the other hand, the two regional discontinuities in the succession, represented by the Piedra Amarilla and Barker surfaces, may have been driven by sea level fall associated with glacial eustacy. In this regard only the upper Barker surface of Ediacaran age is directly associated with the development of phosphorite. Development of thick bedded and economically important phosphorites in the middle Ediacaran Doushantuo Formation of South China are also associated with unconformity surfaces (McFadden et al., 2008; Xiao et al., 2012) that may be eustatic in origin, but their glacial affinity has not been demonstrated. Forced regression and enhanced erosion of continental margins, however, is contrary to the view that the authigenic generation of phosphate is commonly associated with low sediment supply in marine platforms (Föllmi et al., 1991; Cook and Shergold, 2005). Insofar as the phosphorite concretions were developed during subsequent transgression when the continents would be flooded (Poiré, 1993), it is uncertain how glaciation was directly involved in their formation.

On the other hand, post-glacial transgression has been linked to high primary productivity (Hoffman et al., 2012), an expected requirement for phosphorite genesis. In this regard, the negative-to-positive trend in carbon isotopes at the base of the Villa Mónica Formation immediately above the concretionary horizon is consistent with cap carbonates of Neoproteozoic age (Gómez-Peral et al., 2007). Many of the Neoproterozoic glacial diamictites are known to be cemented with iron oxides and to be associated with the accumulation of iron-formation (Derry et al., 1992). We note that there is a close relationship between iron and phosphate in the lower phosphatic horizon of the Villa Mónica Formation, which is a typical feature of Proterozoic phosphorites (Glenn, 1990; Glenn et al., 1994; Baioumy, 2007; Nelson et al., 2010). Whether this potential glacial association is primary or diagenetic (Jarvis et al., 1994; Baioumy, 2007) is unknown, but warrants further exploration.

6.2. Phosphogenesis and sedimentary paleoenvironments

The phosphate deposits of the Villa Mónica Formation are characterized by a close association with stromatolites, similar to other Precambrian occurrences worldwide (Nelson et al., 2010), suggesting the influence of microorganisms during phosphogenesis. Bacterial degradation of organic matter in the cyanobacterial mats was thus likely responsible for local phosphate enrichment in pore waters. Enrichment would subsequently result in the replacement of carbonate by carbonate fluorapatite or francolite (Jahnke et al., 1983; Schenau et al., 2000).

Our environmental model for phosphate genesis during Villa Mónica time is consistent with oceanic stratification in the Neoproterozoic (Fig. 11), which would have resulted in anoxia below the photic zone (Fig. 11). In anoxic environments there would have likely been an increase in ^{13}C depleted alkalinity and phosphorous due to the anaerobic remineralization of photosynthetically derived organic matter. Moreover, under anoxic conditions Ce^{4+} would have been reduced to Ce^{3+} and thus the element would not been preferentially sequestered in phosphate minerals or other oceanic sediments relative to other REEs. Moreover, the release and buildup of phosphorous may be related to a consortium of sulfide oxidizing and sulfate reducing bacteria living in these anoxic environments (Schenau et al., 2000; Asaf et al., 2013) assuming sulfate was readily available. In contrast, the phosphate concretions in the Cerro Negro Formation, which reveal strong negative Ce anomalies, likely formed under oxidized conditions during oceanic transgression, which likely delivered phosphorous from deep water to the marine shelf environment (Fig. 11).

Phosphogenesis is promoted during early diagenesis, when iron is cycled under oxygenated conditions on the bottom water (Pufahl et al., 2003; Nelson et al., 2010; Xiao et al., 2012 and cited therein). The growth of phosphate concretions commonly occurs within decimeters to meters below the sediment–water interface during the suboxic diagenesis of organic-rich mud deposits (Morad and Al-Aasm, 1994; Felitsyn and Morad, 2002). These concretions typically have REE concentrations up to 50–100 times higher than shale-normalized values. The phosphate concretionary levels represented in these two sedimentary sequences of the Tandilia System may have originated in situ due to phosphogenesis during the early diagenetic precipitation of francolite in upwelling areas related to the shallow continental margin associated with relative sea-level changes. Subsequently, the diagenetic process caused by the recrystallization of the initial francolite gave origin to the fluorapatite during burial.

7. Conclusions

In the Tandilia System, two phosphogenic events are recognized in Neoproterozoic strata that may span an age of over 200 Ma, even though they are stratigraphically separated by only about 100 m. The Piedra Amarilla unconformity surface within the succession may occupy much of the missing time. One of the phosphogenic events is represented by the occurrence of phosphate nodules at the base of the Villa Mónica Formation in beds that may record post-glacial transgression. Paleontological and isotopic evidence suggests that this may be earliest Cryogenian in age. The event at the base of the Cerro Negro Formation occurs immediately above an unconformity surface and beds that contain the Ediacaran Period fossil *Cloudina* suggesting a terminal Proterozoic age for these phosphate nodules.

By means of conventional microscopy and SEM images we interpret the nodules to be composed of a cryptocrystalline variety of apatite, which originated as a product of the buildup of phosphorous in organic-rich sediments. The REE patterns of concretions from the Villa Mónica Formation indicate a marine depositional environment under anoxic (positive Ce and Eu anomalies) conditions. On the other hand, phosphorites of the Cerro Negro Formation reveal strongly negative Ce anomalies, but no Eu anomalies, which are consistent with oxygenated conditions associated with the formation of these nodules formed in the Ediacaran–Cambrian boundary succession. This study suggests that marine depositional conditions in which phosphates accumulated were very different in the two discrete stratigraphic levels from the Neoproterozoic of Argentina.

Acknowledgements

The present study was funded by two research grants (to LEGP) provided by the CONICET (PIP-0134) and by the FONCyT (PICT 2012-2798) Argentina. J.M. Canallicchio from Cementos Avellaneda S.A. is kindly acknowledged for providing access to quarries and core information, as well as additional trip support. J. Arrouy is thanked for field assistance and A. Marquez for laboratory SEM-EDAX assistance. J. Maggi, P. García, C. Genazzini, and D. Mártire are thanked for the XRD analysis and thin section preparation. M. Ponce is also thanked for English review. The authors specially thank the two anonymous reviewers and the Editor R. Parrish for their constructive reviews.

References

Aharon, P., Schidlowski, M., Singh, I.B., 1987. Chronostratigraphic markers in the end-Precambrian carbon isotope record of the Lesser Himalaya. Nature 327, 699–701.

Altschuler, Z.S., 1980. The geochemistry of trace elements in marine phosphorites: Part 1. Characteristic abundance and enrichment. In: Bentor, Y.K. (Ed.), Marine Phosphorites SEPM.

Andreis, R.R., Zalba, P.E., Iñiguez Rodriguez, A.M., Morosi, M., 1996. Estratigrafía y evolución paleoambiental de la sucesión superior de la Formación Cerro Largo, Sierras Bayas (Buenos Aires, Argentina). 6° Reunion Argentina de Sedimentología. Actas, 293–298.

Asaf, D., Rotenberg, E., Tatarinov, F., Dicken, U., Montzka, S.A., Yakir, D., 2013. Ecosystem photosynthesis inferred from measurements of carbonyl sulphide flux. Nat. Geosci. 6, 186–190.

Bagnoud-Velásquez, M., Spangenberg, J.E., Poiré, D.G., Gómez-Peral, L.E., 2013. Stable isotopes (C, S) and hydrocarbon biomarkers in Neoproterozoic sediments of the upper section of Sierras Bayas Group, Argentina. Precambrian Res. 231, 340–388.

Baioumy, H., 2011. Rare earth elements and sulfur and strontium isotopes of upper Cretaceous phosphorites in Egypt. Cretac. Res. 32, 368–377.

Baioumy, H.M., 2007. Iron–phosphorus relationship in the iron and phosphorite ores of Egypt. Chem. Erde Geochem. 67, 229–239.

Banerjee, D.M., Schidlowski, M., Arneth, J.D., 1986. Genesis of Upper Proterozoic–Cambrian phosphorite deposits of India: isotopic inferences from carbonate fluorapatite, carbonate andorganic carbon. Precambrian Res. 33, 239–253.

Banerjee, D.M., Schidlowski, M., Siebert, F., Brasier, M.D., 1997. Geochemical changes across the Proterozoic–Cambrian transition in the Durmala phosphorite mine section, Mussoorie Hills, Garhwal Himalaya, India. Paleogeogr. Paleoclimatol. Paleoecol. 132, 183–194.

Barrio, C.A., Poiré, D.G., Iñiguez Rodriguez, A.M., 1991. El contacto entre la Formación Loma Negra (Grupo Sierras Bayas) y la Formación Cerro Negro: un ejemplo de Paleokarst, Olavarría, provincia de Buenos Aires. Revista de la Asociación Geológica Argentina 46 (1–2), 69–76.

Bau, M., Dulski, P., 1996. Distribution of yttrium and rare-earth elements in the Penge and Kuruman iron-formations, Transvaal Suergroup, South Africa. Precambrian Res. 79, 37–55.

Bentor, Y.K., 1980. Phosphorites-the unsolved problems. In: Bentor, Y.K. (Ed.), Marine Phosphorites-Geochemistry, Occurrence, Genesis. Society of Economic Paleontologist and Mineralogists Special Publication 29, Tulsa, pp. 3–18.

Bertram, C.J., Elderfield, H., Aldridge, R.J., Conway Morris, S., 1992. $^{87}Sr/^{86}Sr$, $^{143}Nd/^{144}Nd$ and REEs in Silurian phosphatic fossils. Earth Planet. Sci. Lett. 113, 239–249.

Bertrand-Sarfati, J., Flicoteaux, R., Moussine-Pouchkine, A., Ahmed, A.A.K., 1997. Lower Cambrian apatitic stromatolites and phosphorites related to the glacio-eustatic cratonic rebound (Sahara, Algeria). J. Sediment. Res. 67, 957–974.

Biscaye, P.E., 1965. Mineralogy and sedimentation of recent deep sea clay in the atlantic ocean and adjacent seas and oceans. Geol. Soc. Am. Bull. 76, 803–832.

Blanco, G., Rajesh, H.M., Gaucher, C., Germs, G.J.B., Chemale Jr., F., 2009. Provenance of the Arroyo del Soldado Group (Ediacaran to Cambrian, Uruguay): implications for the paleogeographic evolution of southwestern Gondwana. Precambrian Res. 171, 57–73.

Boggiani, P.C., Gaucher, C., Sial, A.N., Babinski, M., Simon, C.M., Riccomini, C., Ferreira, V.P., Fairchild, T.R., 2010. Chemostratigraphy of the Tamengo Formation (Corumbá Group, Brazil): a contribution to the calibration of the Ediacaran carbon–isotope curve. Precambrian Res. 182, 382–401.

Brasier, M.D., 1992. Background to the Cambrian explosion. J. Geol. Soc. 149, 585–587.

Brindley, G.W., Brown, G., 1980. Crystal Structures of Clay Minerals and Their X-ray Identification. Mineralogical Society, Oxford University, 495 pp.

Canfield, D.E., Poulton, S.W., Knoll, A.H., Narbonne, G.M., Ross, G., Goldberg, T., Strauss, H., 2008. Ferruginous conditions dominated later Neoproterozoic deep-water chemistry. Science 321, 949–952.

Chen, D.F., Dong, W.Q., Qi, L., Chen, G.Q., Chen, X.P., 2003. Possible REE constraints on the depositional and diagenetic environment of Doushantuo Formation phosphorites containing the earliest metazoan fauna. Chem. Geol. 201, 103–118.

Chen, J.Y., Oliveri, P., Gao, F., Dornbos, S.Q., Li, C.W., Bottjer, D.J., Davidson, E.H., 2002. Precambrian animal life: probable developmental and adult cnidarian forms from southwest China. Dev. Biol. 248, 182–196.
Cingolani, C., 2011. The Tandilia System of Argentina as a southern extension of the Río de la Plata craton: an overview. Int. J. Earth Sci. 100, 221–242.
Cingolani, C., Bonhomme, M.G., 1988. Resultados geocronológicos en niveles pelíticos intercalados en las dolomías de Sierras Bayas (Grupo La Tinta), provincia de Buenos Aires. Segundas Jornadas Geológicas Bonaerenses, Buenos Aires, Argentina, pp. 283–289.
Cingolani, C., Rauscher, R., Bonhomme, M.G., 1991. Grupo La Tinta (Precámbrico y Paleozoico inferior), Provincia de Buenos Aires, República Argentina: Nuevos datos geocronológicos y micropaleontológicos en las sedimentitas de Villa Cacique, Partido de Juárez. Revista Técnica de YPFB 12 (2), 177–191.
Cingolani, C.A., Dalla Salda, L., 2000. Buenos Aires cratonic region. In: Cordani, U., Milani, E., Thomaz Filho, A., Campos, D. (Eds.), Tectonic Evolution of South America. 31st International Geological Congress. Rio de Janeiro, pp. 139–146.
Cingolani, C.A., Hartmann, L.A., Santos, J.O.S., McNaughton, N.J., 2002. U–Pb SHIMP dating of zircons from the Buenos Aires Complex of the Tandilia Belt, Rio de La Plata Craton, Argentina. In: Actas XV Congreso Geológico Argentino, El Calafate.
Compton, J.S., Hodell, D.A., Garrido, J.R., Mallinstm, D.J., 1993. Origin and age of phosphorite from the southcentral Florida platform: relation of phosphogenesis to sea-level fluctuations and excursions. Geochim. Cosmochim. Acta 57, 131–146.
Cook, P., 1992. Phosphogenesis around the Proterozoic–Phanerozoic transition. J. Geol. Soc. 149 (4), 615–620.
Cook, P.J., McElhinny, M.W., 1979. A re-evaluation of the spatial and temporal distribution of sedimentary phosphate deposits in the light of plate tectonics. Econ. Geol. 74, 315–330.
Cook, P.J., Shergold, J.H., 1986. Phosphate Deposits of the World. Proterozoic and Cambrian Phosphorites, vol. 1. Cambridge Univ. Press, Cambridge.
Cook, P.J., Shergold, J.H., 2005. Phosphate Deposits of the World. Proterozoic and Cambrian Phosphorites, vol. 1. Cambridge Univ. Press, Cambridge, 386 pp.
Coplen, T.B., Brand, W.A., Gehre, M., Gröning, M., Meijer, H.A., Toman, B., Verkouteren, R.M., 2006. New guidelines for $\delta^{13}C$ measurements. Anal. Chem. 78, 2439–2441.
Derry, L.A., Kaufman, A.J., Jacobsen, S.B., 1992. Sedimentary cycling and environmental change in the late Proterozoic: evidence from stable and radiogenic isotopes. Geochim. Cosmochim. Acta 56, 1317–1329.
Dickson, J.A.D., 1966. Carbonate identification and genesis as revealed by staining. J. Sediment. Petrol. 36, 491–505.
Donnelly, T.H., Shergold, J.H., Southgate, P.N., Barnes, C.J., 1990. Events leading to global phosphogenesis around the Proterozoic/Cambrian transition. In: Notholt, A.J.G., Jarvis, I. (Eds.), Phosphorite Research and Development, vol. 52. Journal Geological Society London Special Publication, pp. 273–287.
Elderfield, H., Graves, M.J., 1982. The Rare earth elements in sea water. Nature 296, 214–219.
Elderfield, H., Pagett, R., 1986. Rare earth elements in Ichthyoliths: variations with redox conditions and depositional environments. Sci. Total Environ. 49, 175–197.
Elderfield, H., Sholkovitz, E.R., 1987. Rare earth elements in the pore waters of reducing nearshore sediments. Earth Planet. Sci. Lett. 82, 280–288.
Esquevin, J., 1969. Influencié de la composition chimique des illites sur leer cristallinite. Bull. Cetre Rech. Pau-SNPA 3 (1), 147–153, Earth Planetary Science Letters 147, 1–7.
Felitsyn, S., Morad, S., 2002. REE patterns in latest Neoproterozoic–early Cambrian phosphate concretions and associated organic matter. Chem. Geol. 187, 257–265.
Filippelli, G.M., Delaney, M.L., 1994. The oceanic phosphorus cycle and continental weathering during the Neogene. Paleoceanography 9, 643–652.
Föllmi, K.B., Garrison, R.E., Grimm, K.A., 1991. Stratification in phosphate sediments: illustrations from Neogene of California. In: Einsele, G., Ricken, W., Seiacher, A. (Eds.), Cycles and Events in Stratigraphy. Springer-Verlag, Berlin, Heidelberg, pp. 492–507.
Frei, R., Gaucher, C., Stolper, D., Canfield, D.E., 2013. Fluctuations in late Neoproterozoic atmospheric oxidation – Cr isotope chemostratigraphy and iron speciation of the late Ediacaran lower Arroyo del Soldado Group (Uruguay). Gondwana Res. 23, 797–811.
Gaucher, C., Poiré, D.G., Gómez-Peral, L.E., Chiglino, L., 2005. Litoestratigrafía, bioestratigrafía y correlaciones de las sucesiones sedimentarias del Neoproterozoico-Cámbrico del Cratón del Río de La Plata (Uruguay y Argentina). Latin Am. J. Sedimentol. Basin Anal. 12 (2), 145–160.
Gaucher, C., Finney, S.C., Poiré, D.G., Valencia, V.A., Grove, M., Blanco, G., Pamoukaghlian, L., Poiré, L.G., 2008. Detrital zircon ages of Neoproterozoic sedimentary successions in Uruguay and Argentina: insights into the geological evolution of the Rio de la Plata Craton. Precambrian Res. 167, 150–170.
Gaucher, C., Germs, G.J.B., 2009. Skeletonised metazoans and protists. Neoproterozoic-Cambrian biota. In: Gaucher, C., Sial, A.N., Halverson, G.P., Frimmel, H.E. (Eds.), Neoproterozoic-Cambrian Tectonics, Global Change and Evolution: a focus on southwestern Gondwana. Developments in Precambrian Geology, vol. 16. Elsevier, pp. 327–338.
Gaucher, C., Poiré, D.G., 2009a. Biostratigraphy. Neoproterozoic–Cambrian Evolution of the Rio de la Plata Palaeocontinent. In: Gaucher, C., Sial, A.N., Halverson, G.P., Frimmel, H.E. (Eds.), Neoproterozoic–Cambrian Tectonics, Global Change and Evolution: A focus on Southwestern Gondwana. Elsevier, pp. 103–114.
Gaucher, C., Poiré, D.G., 2009b. Paleoclimatic events. Neoproterozoic–Cambrian evolution of the Río de la Plata Palaeocontinent. In: Gaucher, C., Sial, A.N., Halverson, G.P., Frimmel, H.E. (Eds.), Neoproterozoic–Cambrian Tectonics, Global Change and Evolution: A Focus on Southwestern Gondwana. Development in Precambrian Geology. Elsevier, pp. 123–130.
Gaucher, C., Sial, A.N., Poiré, D.G., Gomez Peral, L., Ferreira, V.P., Pimentel, M.M., 2009. Chemostratigraphy, Neoproterozoic–Cambrian evolution of the Rio de la Plata Palaeocontinent. In: Gaucher, C., Sial, A.N., Halverson, G.P., Frimmel, H.E. (Eds.), Neoproterozoic–Cambrian Tectonics, Global Change and Evolution: A Focus on Southwestern Gondwana. Developments in Precambrian Geology. Elsevier, Amsterdam, pp. 115–122.
German, C.R., Elderfield, H., 1990. Application of the Ce anomaly as paleoredox indicator: the ground rules. Paleoceanography 5, 823–833.
Germs, G.J.B., Gaucher, C., 2012. Nature and extent of a late Ediacaran (ca. 547 Ma) glacigenic erosion surface in southern Africa. South Afr. J. Geol. 115, 91–102.
Glenn, C.R., 1990. Depositional sequence of the Duwi, Sibaiya and Phosphate Formations, Egypt: phosphogenesis and glauconitization in a late Cretaceous epeiric sea. In: Notholt, A.J.G., Jarvis, I. (Eds.), Phosphorite Research and Development. Geololical Society Special Publication 52, pp. 205–222.
Glenn, R.C., Follmi, K.B., Riggs, S.R., Baturin, G.N., Grimm, K.A., Trappe, J., Abed, A.M., Galli-Olivier, C., Garrison, R.E., Ilyin, A., Jehl, C., Roharlich, V., Sadaqah, R.M., Schidlowski, M., Sheldon, R.E., Siegmund, H., 1994. Phosphorus and phosphorites: sedimentology and environments of formation. Eclogae Geol. Helv. 87, 747–788.
Gómez-Peral, L.E., Poiré, D.G., Strauss, H., Zimmermann, U., 2007. C—O isotope data and diagenetic constraints of the Neoproterozoic Sierras Bayas Group (SW Gondwana), Argentina. Chem. Geol. 237, 127–146.
Gómez-Peral, L.E., Raigemborn, M.S., Poiré, D.G., 2011. Petrología y evolución diagenética de las facies silicoclásticas del Grupo Sierras Bayas, Sistema de Tandilia, Argentina. Latin Am. J. Sedimentol. Basin Anal. (LAJSBA) 18 (1), 3–41.
Gómez-Peral, L.E., Sial, A.N., Poiré, D.G., Kaufman, A.J., Arrouy, J., 2012. C—O—Sr isotope stratigraphy of the Neoproterozoic carbonate Successions of the Sierras Bayas Group, Río de La Plata Craton, Argentina: palaeoclimatic implications. In: The Neoproterozoic Era: Evolution, Glaciations, Oxygenation, 19–21 September 2012, London, England, Abstract Book, pp. 128–129.
Grandjean, P., Cappetta, H., Albarède, F., 1988. The REE and Nd of 40–70 Ma old fish debris from the West-African platform. Geophys. Res. Lett. 15, 389–392.
Grandjean, P., Cappetta, H., Michard, A., Albarède, F., 1987. The assessment of REE patterns and $^{143}Nd/^{144}Nd$ ratios in fish remains. Earth Planet. Sci. Lett. 84, 181–196.
Halverson, G.P., Wade, B.P., Hurtgen, M.T., Barovich, K.M., 2010. Neoproterozoic chemostratigraphy. Precambrian Res. 182, 337–350.
Hannigan, R.E., Sholkovitz, E.R., 2001. The development of middle rare earth element enrichments in freshwaters: weathering of phosphatic minerals. Chem. Geol. 175, 495–508.
Hartmann, L.A., Santos, J.O.S., Cingolani, C.A., McNaughton, N.J., 2002. Two paleoproterozoic orogenies in the evolution of the tandilia belt, Buenos Aires, as evidenced by zircon U–Pb shrimp geochronology. Int. Geol. Rev. 44, 528–543.
Hoffman, P.F., Hawkins, D.P., Isachsen, C.E., Bowring, S.A., 1996. Precise U–Pb zircon ages for early Damaran magmatism in the Summas Mountains and Welwitschia inlier, northern Damara belt. Namibia: Geol. Surv. Namibia Commun. 11, 47–52.
Hoffman, P.F., Halverson, G.P., Domacke, E.W., Malooff, A.C., Swanson-Hysellf, N.L., Cox, G.M., 2012. Cryogenian glaciations on the southern tropical paleomargin of Laurentia (NE Svalbard and East Greenland), and a primary origin for the upper Russøya (Islay) carbon isotope excursion. Precambrian Res. 206–207, 137–158.
Holser, W.T., 1997. Evaluation of the application of rare-earth elements to paleoceanography. Palaeogeogr. Palaeoclimatol. Palaeoecol. 132, 309–323.
Ilyin, A.V., 1998. Rare-earth geochemistry of 'old' phosphorites and probability of syngenetic precipitation and accumulation of phosphate. Chem. Geol. 144, 243–256.
Jahnke, R.A., Emerson, S.R., Roe, K.K., Burnett, W.C., 1983. The present day formation of apatite in Mexican continental margin sediments. Geochim. Cosmochim. Acta 47, 259–266.
Jarvis, I., Burnett, W.C., Nathan, Y., Almbaydin, S.M.F., Attia, A.K.M., Castro, L.N., Flicoteaux, R., Hilmy, M.E., Husain, V., Qutawah, A.A., Serjani, A., Zanin, Y.N., 1994. Phosphorite geochemistry: State-of-the-art and environmental concern. In: Concepts and Controversies in Phosphogenesis. Proceedings of the Symposium and Workshop Held on 6–10 September 1993, Switzerland, pp. 643–700.
Jiang, G., Shi, X., Zhang, S., Wang, Y., Xiao, S., 2011. Stratigraphy and paleogeography of the Ediacaran Doushantuo Formation (ca. 635–551 Ma) in South China. Gondwana Res. 19, 831–849.
Kaufman, A.J., Jacobsen, S.B., Knoll, A.H., 1993. The Vendian record of Sr and C isotope variation in seawater: implications for tectonic and paleoclimate. Earth Planet. Sci. Lett. 120, 409–430.
Kaufman, A.J., Knoll, A.H., Semikhatov, M.A., Grotzinger, J.P., Jacobsen, S.B., Adams, W., 1996. Integrated chemostratigraphy of Proterozoic–Cambrian boundary beds in the western Anabar region, northern Siberia. Geol. Mag. 133, 509–533.
Kaufman, A.J., Sial, A.N., Frimmel, H.E., Misi, A., 2009. Neoproterozoic to Cambrian palaeoclimatic events in southwestern Gondwana. In: Gaucher, C., Sial, A.N., Halverson, G.P., Frimmel, H.E. (Eds.), Neoproterozoic-Cambrian Tectonics, Global Change and Evolution: a focus on southwestern Gondwana, vol. 16. Elsevier. Develop. Precambrian Geol., pp. 369-388.
Kawashita, K., Varela, R., Cingolani, C., Soliani Jr., E., Linares, E., Valencio, S.A., Ramos, A.V., Do Campo, M., 1999. Geochronology and Chemostratigraphy of "La Tinta" Neoproterozoic Sedimentary rocks, Buenos Aires Province, Argentina. In: II South American Symposium on Isotope Geology, Brazil, pp. 403–407.

Kimura, H., Matsumoto, R., Kakuwa, Y., Hamdi, B., Zibaseresht, H., 1997. The Vendian–Cambrian $\delta^{13}C$ record, North Iran: evidence for overturning of the ocean before the Cambrian explotion. Earth Planet. Sci. Lett. 147, 1–7.
Knoll, A.H., Hayes, J.M., Kaufman, A.J., Swett, K., Lambert, I.B., 1986. Secular variation in carbon isotope ratios from Proterozoic succession of Svalbard and East Greenland. Nature 321, 832–838.
Kolodny, Y., 1981. Phosphorites. In: Emiliani, C. (Ed.), The Sea, VII, The Oceanic Lithosphere. Wiley Interscience, New York, pp. 981–1023.
Kolodny, Y., Luz, B., 1992. Phosphate deposits, formation and diagenetic history. In: Clauer, N., Chaudhuri, S. (Eds.), Isotopic Signatures and Sedimentary Records. Springer Verlag, pp. 69–122.
Kubler, B., 1967. La cristallinité de Illité et les zones tout á fair supérieures du métamorphisme. In: Etages Tectoniques-Colloque de Neuchâtel, Switzerland., pp. 105–122.
Laenen, B., Hertogen, J., Vandenbarghe, N., 1997. The variation of the trace-element content of the fossil biogenic apatite through eustatic sea level cycles. Paleogeogr. Paleoclimatol. Paleoceanogr. 132, 325–342.
Leanza, C.A., Hugo, C.A., 1987. Descubrimiento de fosforitas sedimentarias en el Proterozoico Superior de Tandilia, Buenos Aires, Argentina. Revista de la Asociación Geológica Argentina 42 (3–4), 417–428.
Li, C., Love, G.D., Lyons, T.W., Fike, D.A., Sessions, A.L., Chu, X., 2010. A stratified redox model for the Ediacaran ocean. Science 328, 80–83.
Liu, Y.G., Miah, M.R.V., Schmitt, R.A., 1988. Cerium: a chemicaltracer for paleo oceanic conditions. Geochim. Cosmochim. Acta 52, 1361–1371.
Lécuyer, C., Grandjean, P., Barrat, J., Nolvak, J., Emig, C., Paris, F., 1998. 18O and REE contents of phosphatic brachiopods: a comparison between modern and lower Paleozoic populations. Geochim. Cosmochim. Acta 62, 2429–2436.
Logan, G.A., Hayes, J.M., Hieshima, G.B., Summons, R.E., 1995. Terminal Proterozoic reorganization of biogeochemical cycles. Nature 376, 53–56.
Marchesse, H.G., Di Paola, E., 1975. Miogeosinclinal Tandil. Revista de la Asociación Geológica Argentina 30 (2), 161–179.
Mazumdar, A., Banerjee, D.M., Schidlowski, M., Balaram, V., 1999. Rare-earth elements and Stable Isotope Geochemistry of early Cambrian chert-phosphorite assemblages from the Lower Tal Formation of the Krol Belt (lesser Himalaya, India). Chem. Geol. 156, 275–279.
McArthur, J.M., 1985. Francolite geochemistry-compositional controls during formation, diagenesis, metamorphism and weathering. Geochim. Cosmochim. Acta 49, 23–35.
McArthur, J.M., Hamilton, P.J., Greensmith, J.T., Boyce, A.J., Fallick, A.E., Birch, G., Walsh, J.N., Benmore, R.A., Coleman, M.L., 1987. Phosphorite geochemistry: isotopic evidence for meteoric alteration of francolite on a local scale. Chem. Geol. 65, 415–425.
McArthur, J.M., Walsh, J.N., 1984. Rare-earth element geochemistry of the phosphorites. Chem. Geol. 47, 191–220.
McFadden, K.A., Huang, J., Chu, X., Jiang, G., Kaufman, A.J., Zhou, C., Yuan, X., Xiao, S., 2008. Pulsed oxidation and bioloical evolution in the Ediacaran Doushantuo Formation. Proc. Natl. Acad. Sci. U. S. A. 105 (9), 3197–3202.
McLennan, S.M., 1989. Rare earth elements in sedimentary rocks: influence of provenance and sedimentary processes. In: Lipin, B.R., McKay, G.A. (Eds.), Geochemistry and Mineralogy of Rare Earth Elements, vol. 21. Min. Soc. Am. Rev. Mineral, pp. 169–200.
Melezhik, V.A., Fallick, A.E., Rychanchik, D.V., Kuznetsov, A.B., 2005. Palaeoproterozoic evaporites in Fennoscandia: implications for seawater sulfate, $\delta^{13}C$ excursions and the rise of atmospheric oxygen. Terra Nova 17, 141–148.
Misi, A., Kyle, J.R., 1994. Upper Proterozoic carbonate stratigraphy, diagenesis and stromatolitic phosphorite formation, Irece Basin, Bahia, Brazil. J. Sediment. Res. 64, 299–310.
Moore, D., Reynolds Jr., R., 1989. X-ray Diffraction and The Identification and Analysis of Clay Minerals. Oxford, New York, 332 pp.
Morad, S., Al-Aasm, I.S., 1994. Conditions of formation and diagenetic evolution of Upper Proterozoic phosphate nodules from southern Sweden: evidence from petrology, mineral chemistry and isotopes. Sediment. Geol. 88, 267–282.
Morad, S., Felitsyn, S., 2001. Identification of primary Ce-anomaly signatures in fossil biogenic apatite: implication for the Cambrian oceanic anoxia and phosphogenesis. Sediment. Geol. 143, 259–264.
Murray, R.W., Buchholtz, M.R., Gerlach, D.C., Russ III, G.P., Jones, D.L., 1992. Rare earth, major, and trace element composition of Monterey and DSDP chert and associated host sediments: assessing the influence of chemical fractionation during diagenesis. Geochim. Cosmochim. Acta 56, 2657–2671.
Nathan, Y., Nielsen, H., 1980. Sulfur isotopes in phosphorites. In: Bentor, Y.K. (Ed.), Marine Phosphorites. SEPM Special Publication 29, pp. 73–78.
Nelson, G.J., Pufahl, P.K., Hiatt, E.E., 2010. Paleoceanographic constraints on Precambrian phosphorite accumulation, Baraga Group, Michigan, USA. Sediment. Geol. 226, 9–21.
Notholt, A.J.G., Sheldon, R.P., Davidson, D.F., 1989. Phosphate Deposits of the World. Phosphate Rock Resources, vol. 2. Cambridge Univ. Press, Cambridge, 566 pp.
O'Brien, G.W., Veeh, H.H., 1983. Are phosphorites reliable indicators of upwelling? In: Suess, E., Thiede, J. (Eds.), Coastal Upwelling, Its Sediment Record. Plenum Press, New York, pp. 399–419.
Pankhurst, R.J., Ramos, A., Linares, E., 2003. Antiquity of the Río de la Plata craton in Tandilia, southern Buenos Aires province, Argentina. J. South Am. Earth Sci. 16, 5–13.
Picard, P., Lécuyer, C., Barrat, J.-A., Garcia, J.-P., Dromart, G., Sheppard, S.M.F., 2002. Rare earth element contents of Jurassic fish and reptile teeth and their potential relation to seawater composition (Anglo-Paris Basin, France and England). Chem. Geol. 186, 1–16.
Poiré, D.G., (Unpublished PhD Tesis) 1987. Mineralogía y sedimentología de la Formación Sierras Bayas en el Núcleo Septentrional de las sierras homónimas, partido de Olavarría, provincia de Buenos Aires. 494, Facultad de Ciencias Naturales y Museo, Universidad Nacional de La Plata, 271 pp.
Poiré, D.G., 1989. Stromatolites of the Sierras Bayas Group, Upper Proterozoic of Olavarría, Sierras Septentrionales, Argentina. Stromat. Newsl. 11, 58–61.
Poiré, D.G., 1993. Estratigrafía del Precámbrico sedimentario de Olavaría, Sierras Bayas, Provincia de Buenos Aires, Argentina. In: XII Congreso Geológico Argentino y II Congreso de Exploración de Hidrocarburos Act. II, pp. 1–11.
Poiré, D.G., 2012a. The Neoproterozoic stromatolites from Villa Mónica Formation (Sierras Bayas Group) Tandilia System: the oldest life record from Argentina. In: The Neoproterozoic Era: Evolution, Glaciations, Oxygenation, 19–21 September, Londres, Inglaterra, Abstract Book, p. 133.
Poiré, D.G., 2012b. The Neoproterozoic sedimentary record from Tandilia System, Argentina. In: The Neoproterozoic Era: Evolution, Glaciations, Oxygenation, 19–21 September, London, England, Abstract Book, p. 132.
Poiré, D.G., Spalletti, L.A., del Valle, A., 2003. The Cambrian–Ordovician siliciclastic platform of the Balcarce Formation (Tandilia System, Argentina): facies, trace fossils, palaeoenvironments and sequence stratigraphy. Geol. Acta 38, 41–60.
Poiré, D.G., Spalletti, L.A., 2005. La cubierta sedimentaria precámbrica/paleozoica inferior del Sistema de Tandilia. In: De Barrio, R.E., Etcheverry, R.O., Caballé, M.F., Llambías, E.J. (Eds.), Geología y Recursos Minerales de la provincial de Buenos Aires. Relatorio del XVI Congreso Geológico Argentino, La Plata, pp. 51–68.
Poiré, D.G., Gaucher, C., Germs, G., 2007. La superficie "Barker" y su importancia regional, Neoproterozoico del Cratón del Río de La Plata. In: VI Jornadas Geológicas y Geofísicas Bonaerenses, Actas: 36, Mar del Plata, Argentina.
Pöthe de Baldis, D., Cuomo, J., 1983. Los fósiles precámbricos de la Formación Sierras Bayas (Olavarría) y su importancia intercontinental. Revista de la Asociación Geológica Argentina 38, 73–83.
Praekelt, H.E., Germs, G.J.B., Kennedy, J.H., 2008. A distinct unconformity in the Cango Caves Group of the Neoproterozoic to early Paleozoic Saldania Belt in South Africa: its regional significance. South Afr. J. Geol. 111, 357–368.
Pufahl, P.K., Grimm, K.A., Abed, A.M., Sadaqah, R.M.Y., 2003. Upper Cretaceous (Campanian) phosphorites in Jordan: Implications for the formation of south Tethyan phosphorite giant. Sediment. Geol. 161, 175–205.
Rapalini, A., Trindade, R.I., Poiré, D.G., 2013. The La Tinta pole revisited: Paleomagnetism of the Neoproterozoic Sierras Bayas Group (Argentina) and its implications for Gondwana and Rodinia. Precambrian Res. 224, 51–70.
Rapela, C.W., Pankhurst, R.J., Casquet, C., Fanning, C.M., Baldo, E.G., González-Casado, J.M., Galindo, C., Dahlquist, J., 2007. The Río de la Plata Craton and the assembly of SW Gondwana. Earth Sci. Rev. 83, 49–82.
Reynard, B., Lecuyér, C., Grandjean, P., 1999. Crystal–chemical controls on rare-earth element concentrations in fossil biogenic apatites and implications for paleoenvironmental reconstructions. Chem. Geol. 155, 233–241.
Sadaqah, M.R., Abed, M.A., Grimm, A.K., Pufahl, K.P., 2007. Oxygen and carbon isotopes in Jordanian phosphorites and associated fossils. J. Asian Earth Sci. 29, 803–812.
Schenau, S.J., Slomp, C.P., De Lange, G.J., 2000. Phosphogenesis and active phosphorite formation in sediments from the Arabian Se oxygen minimun zone. Mar. Geol. 169, 1–20.
Semikhatov, M.A., 1975. Experiences in stromatolite studies in the USSR. In: Walter, M.R. (Ed.), Stromatolites. Elsevier, Amsterdam, pp. 337–357.
Semikhatov, M.A., 1991. General problems of Proterozoic stratigraphy in the URSS. Sov. Sci. Rev. Geol. Sect. 1, 1–192.
Sheldon, R.P., 1980. Episodicity of phosphate deposition and deep ocean circulation – a hypothesis. In: Bentor, Y.K. (Ed.), Marine Phosphorites – Geochemistry, Occurrence, Genesis. Sot. Econ. Paleontol. Mineral. Spec. Publ. 29, pp. 239–247.
Sheldon, R.P., 1981. Ancient marine phosphates. Annu. Rev. Earth Planet. Sci. 9, 251–284.
Shemesh, A., Kolodny, Y., Luz, B., 1988. Isotope geochemistry of oxygen and carbon in phosphate and carbonate of phosphorite francolite. Geochim. Cosmochim. Acta 52, 2565–2572.
Shields, G., Stille, P., 2001. Diagenetic constraints on the use of cerium anomalies as palaeoseawater redox proxies: an isotopic and REE study of Cambrian phosphorites. Chem. Geol. 175, 29–48.
Sholkovitz, E., Landing, W.M., Lewis, B.L., 1994. Ocean particle chemistry: the fractionation of the rare earth elements between suspended particles and seawater. Geochim. Cosmochim. Acta 58, 1567–1580.
Spalletti, L.A., Poiré, D.G., 2000. Secuencias silicoclásticas y carbonáticas del Precámbrico y Paleozoico inferior del Sistema de Tandilia, Argentina. In: II Congreso Latinoamericano de Sedimentología y VIII Reunión Argentina de Sedimentología, Guía de Campo, pp. 19–30, 39 pp. Special Publication 29.
Spotl, C., 2011. Long-term performance of the Gasbench isotope ratio mass spectrometry 828 system for the stable isotope analysis of carbonate microsamples. Rapid 829 Commun. Mass Spectrom. 25, 1683–1685.
Stern, R.J., Mukherjee, S.K., Miller, N.R., Ali, K., Johnson, P.R., 2013. ~750 Ma banded iron formation from the Arabian-NubianShield – implications for understanding Neoproterozoic tectonics, volcanism, and climate change. Precambrian Res. 239, 79–94.
Taylor, S.R., McLennan, S.M., 1985. The Continental Crust: Its Composition and Evolution. Oxford (Blackwell Scientific).
Tissot, B., 1979. Effects on profilic petroleum source rocks and major coal deposits caused by sea level changes. Nature 277, 463–465.
Vail, P.R., Mitchum Jr., R.M., Thompson III, S., 1977. Seismic stratigraphy and global changes of sea level. In: Payton, C.E. (Ed.), Seismic Stratigraphy – Applications

to Hydrocarbon Exploration. American Association of Petroleum Geologists, Momoir 26, Tulsa, pp. 83–97.
Wright, J., Schrader, H., Holser, W.T., 1987. Paleoredox variations in ancient oceans recorded by rare earth elements in fossil apatite. Geochim. Cosmochim. Acta 51, 613–644.
Wright, J., Seymour, R.S., Shaw, H.F., 1984. REE and Nd isotopes in conodont apatite: variations with geological age and depositional environment. In: Clark, D.L. (Ed.), Conodont Biofacies and Provinciales, vol. 196. Geol. Soc. Am. Spec. Paper, pp. 325–340.
Xiao, S., McFaddenb, K.A., Peekc, S., Kaufmand, A.J., Zhou, C., Jiangf, G., Hug., J., 2012. Integrated chemostratigraphy of the Doushantuo Formation at the northern Xiaofenghe section (Yangtze Gorges, South China) and its implication for Ediacaran stratigraphic correlation and ocean redox models. Precambrian Res. 192–195, 125–141.
Yang, J., Sun, W., Wang, Z., Xue, Y., Tao, X., 1999. Variations in Sr and C isotopes and Ce anomalies in successions from China: evidence for the oxygenation of Neoproterozoic seawater. Precambrian Res. 93, 215–233.
Zalba, P.E., Poiré, D.G., Andreis, R., Iñiguez, A.M., 1992. Precambrian paleoweathering records and paleosurfaces of Tandilia System, Buenos Aires Province, Argentina. In: Schmit, J., Gall, Q. (Eds.), Mineralogical and Geochemical Records of Paleoweathering. ENSMP Memories des Sciences de la Terre, vol. 18, pp. 153–161.
Zimmermann, U., Poiré, D.G., Gómez-Peral, L.E., 2011. Neoproterozoic to Lower Palaezoic successions of Tandilia System in Argentina: implication for the palaeotectonic framework of southwest Gondwana. Int. J. Earth Sci. 100, 489–510.